THE OPTIMIZATION AND USE OF A PHOTON COUNTING SYSTEM FOR THERMOLUMINESCENT DOSIMETRY

by

BRIAN KENNETH HARMS

B.S., Kansas State University, 1980

A MASTER'S THESIS

submitted in partial fulfillment of the

requirements for the degree

MASTER OF SCIENCE

Department of Nuclear Engineering

KANSAS STATE UNIVERSITY
Manhattan, Kansas

1982

Approved by:

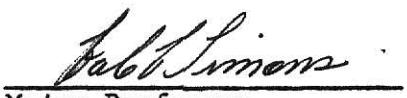

Major Professor

TABLE OF CONTENTS

TABLE OF CONTENTS

LIST OF FIGURES

LIST OF FIGURES

LIST OF TABLES

1.0 Introduction

As a result of the growth of nuclear power generation and other radiation related industries such as medicine, it has become increasingly important to have a reliable and accurate means of measuring relatively small absorbed doses. Personnel dosimetry requires accurate measurement and records of the doses received by workers involved with radioactive materials. Environmental monitoring requires the measurement of virtual background levels (approximately 0.01 mR/h) of radiation near nuclear reactors or other potential sites of low level radiation.

Until recently, these types of measurements have been made with photographic emulsions (film badges) (1). The sensitivity and properties of these film badges can be controlled by their composition and processing, enabling them, in principle, to detect most types of radiation. Presently there is a major shift from film badges to the more convenient thermoluminescence dosimeters (TLDs), especially for personnel monitoring. By varying the composition and encapsulating materials, TLDs can be used for gamma, beta, and neutron dosimetry. TLD response to other types of ionizing radiation such as heavy charged particles has also been investigated (2-5).

The advantages of TLDs include: high sensitivity, good reproducibility, relative insensitivity to humidity and temperature, and convenience of analysis. In regard to convenience of analysis, most TLDs are read out on the job site in less than a minute, whereas it is necessary to send the photographic emulsions to a separate laboratory for analysis.

The useful dose range of TLDs is usually estimated to be about 10^{-3} - 10^{5} rads for LiF and 10^{-3} - 10^{6} rads for CaF_2:Mn (6). Other authors have reported the capability of measuring lower doses (the lowest is 0.1 mrad (7)), but these results are usually based on extrapolations from data for doses greater than 1.0 rad and often contain erroneous assumptions such as the absence of chemiluminescence and the validity of a Poisson statistical model for the light detector's output pulses. The experimentally determined minimum detectable dose reported in the literature was 0.2 mrad ± 20% or 0.5 mrad ± 30% (8).

Evaluating the dose received by a TLD consists of measuring the amount of light emitted when it is heated. The light output is nearly always measured with a photomultiplier tube (PMT), the most sensitive known light detector. Although researchers have occasionally measured the PMT output by counting pulses, the great majority of light detection has been done using the charge integration (or DC) technique. However, recent developments in high-speed digital electronics have rekindled interest in the use of pulse or photon counting for low level light measurements.

The purpose of this work was to extend the initial work reported by D.W. Hanna (9) through design changes to the first photon counting system built at Kansas State University and to investigate means of improving the system's performance at the upper and lower ends of its useful dose range.

2.0 Thermoluminescence Dosimeters

2.1 The Band Theory Model

Although TLDs have been in use for many years, the complex mechanisms of thermoluminescence (TL) in specific dosimeter materials is still not completely understood.

A simple approach to thermoluminescence which illustrates the basic principles is the band theory model (10). Figure 2-1 shows the energy band structure for a dosimeter crystal. All bound electrons are contained in the valence band. The conduction band contains free electrons which may migrate in the crystal lattice. In an ideal crystal the forbidden gap effectively isolates the conduction and valence bands. In a real crystal, defects allow for intermediate energy levels as shown in Fig. 2-1. Level E represents an electron trap and H a hole trap. The recombination of holes and electrons may occur at L, a luminescence center. This recombination at level L results in photon emission.

The thermoluminescence process occurs as follows: Ionizing radiation absorbed in the crystal moves electrons from the valence band to the conduction band where they are free to move through the crystal. Likewise, the corresponding holes which are formed are free to move through the valence band. If trapping levels such as E and H are present, the electrons and holes may be trapped producing electron and hole centers. Hole centers are often thermally unstable and may decay rapidly at room temperature. The trapped electrons will remain in their traps until they acquire enough energy to escape. This energy may be supplied by elevating the crystal temperature. When the electrons

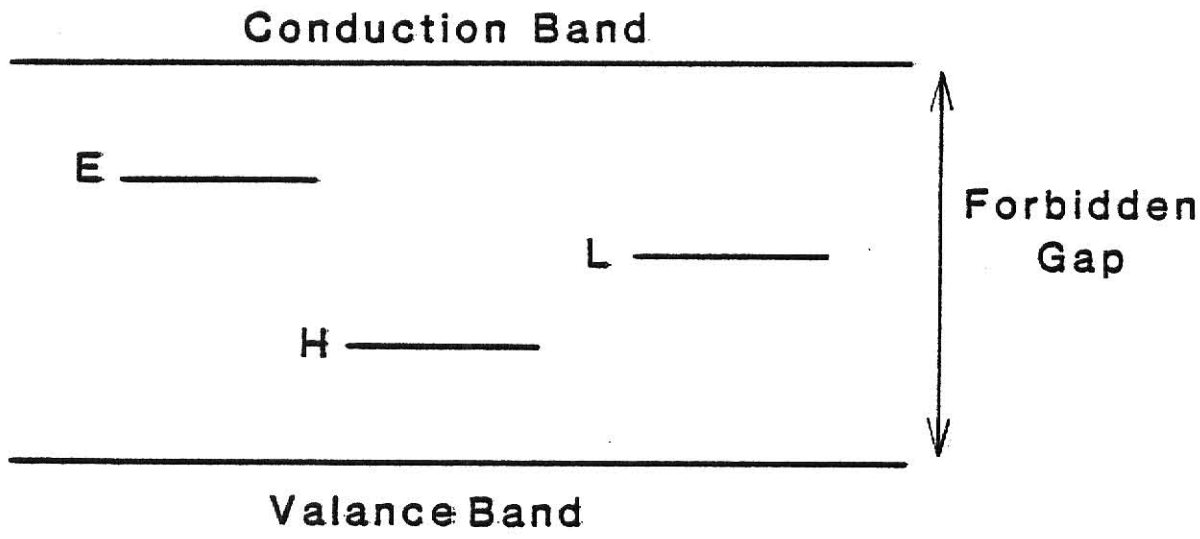

Fig. 2-1. Energy band diagram for a TLD crystal with electron traps (E), hole traps (H), and luminescence centers (L) (10).

acquire sufficient thermal energy they will be released and may recombine with holes at luminescence centers, in which case the excess energy is radiated as visible or ultraviolet photons. Other modes of recombination which result in either immediate fluorescence or thermal degradation with no luminescence are also possible.

2.2 Glow Peaks and Annealing

To free a TLD from any past irradiation history it must be given a pre-irradiation anneal of 1 hr. at 400°C. If the TLD is then cooled and irradiated, its thermoluminescence (glow) intensity upon heating will be a function of temperature. A plot of glow intensity as a function of temperature will reveal at least six glow peaks between room temperature and 300°C for LiF TLDs. These peaks all have finite half-lives ranging from 10 min. for the lowest temperature peak to hundreds of years for the highest temperature peak (10). The fifth peak - occurring somewhere around 170°-210°C depending on the heating rate - is the one commonly used for dosimetry. It has an approximate half-life of 80 years.

If the 400°C anneal is followed by a 2 hr. anneal at 100°C, the traps associated with the low temperature glow peaks may be significantly reduced. In addition, if a post-irradiation anneal of 10 min. at 100°C is employed to accelerate the fading in the remaining low temperature peaks, virtually all the TL from the low temperature peaks may be eliminated before readout. This is desirable because the low temperature peaks are not normally used to obtain dosimetric information and only add noise to the useful portion of the glow curve.

Once the glow curve has been obtained, there are two methods available for determining the dose received by the TLD. The first is based on the fact that the area under the glow peak is proportional to the absorbed dose. A temperature window containing the dosimetric peak is selected, and the TL emitted between these temperatures is integrated to obtain the output. The second method consists of simply measuring the glow-peak height since this parameter is also proportional to the absorbed dose.

2.3 Non-radiation Induced TL

In addition to the TL caused by the irradiation of a TLD, the readout cycle also produces some non-radiation-induced TL. This light emission is usually attributed to triboluminescence or chemiluminescence of the TLD. Triboluminescence is caused by almost any form of mechanical disturbance of the phospher grains, especially in powders where grinding or sieving has been used. Triboluminescence is usually negligible for TLDs in extruded ribbon or rod form but may be noticeable in the presence of severe vibrations (10).

Chemiluminescence is believed to be caused by the oxidation of dirt which has been trapped on the surface of the dosimeter. This effect may be greatly reduced by performing the readout in an inert atmosphere.

Nitrogen is most commonly used because it is relatively inexpensive. Care should be taken to ensure the gas is free of oxygen, water vapor, and dust. Driscoll and McKinlay have also reported a reduction in chemiluminescence obtained by washing the TLDs in acidic methanol(11).

They observed that using nitrogen gas during readout reduced the background by 50% while washing the TLDs reduced the background to 10% of its original value (without the use of nitrogen gas).

The heating tray (or planchet) is also a source of detrimental background in the form of infrared thermal glow. This noise component may be reduced by use of a filter which blocks light at the infrared wavelengths but passes the blue light of the TLDs. (The wavelengths of maximum light emission are approximately 400 nm for LiF and 500 nm for CaF_2:Mn.)

2.4 Supralinearity, Sensitization, and Fading

The response of a LiF TLD is linear with respect to dose up to approximately 300 - 1000 rads. At this point the response becomes supralinear and remains so until saturation is reached. Increasing the dose past saturation causes the response to fall off rapidly and doses exceeding 10^6 rads can cause permanent damage to the TLD.

Large doses may be used to an advantage, however, in a process known as irradiation sensitization (10). A typical sensitization process begins with a dose of 3×10^4 - 10^5 rads which is followed by a 50 min. - 4 hr. anneal at 280-300°C. This results in a four to six fold increase in sensitivity. Annealing at temperatures above 360°C eliminates the sensitization effect. This process increases the TLD sensitivity but also produces a high residual background signal which has precluded its use at low doses. Although the background has been prohibitive in the past, it has recently been found that the background may be effectively reduced by annealing the TLDs in the presence of

ultraviolet light (12-14). Jones (14) has reported that a sensitization exposure of $8x10^4$ R followed by a 290°C - 50 min. anneal in the presence of 254 nm ultraviolet light has other advantages in addition to increasing the sensitivity by a factor of 3.8. The observed advantages were: wider linear range, less dependence on the irradiation energy, reduced fading when oven preannealing was not used, no sensitivity reduction after 100 read cycles (the unsensitized TLDs experienced a 10% decrease), and sensitized TLDs were more uniform when calibrated and retained calibration factors more successfully than their unsensitized counterparts.

It has been postulated that a disadvantage of the sensitization process is it will interfere with any attempts at re-evaluating the dose received by the TLD since both processes employ ultraviolet irradiation. An analysis of this alleged disadvantage follows. Re-assessment of absorbed dose depends on a phenomenon known as phototransfered thermoluminescence (PTTL), described below. If a TLD is irradiated with ultraviolet light after it has been read out, charge carries may be released from deep traps related to the absorbed dose which were not dumped during the readout cycle. These carriers may then be retrapped in the dosimetric peak. Repeating the readout procedure will then result in a signal which can be related to the absorbed dose.

Mistry and Khan (13) investigated the compatability of re-assessment and sensitization and found that they apparently depend on different trapping centers and are therefore not mutually exclusive. They measured a factor of three increase in minimum detectable dose using sensitized TLDs but pointed out that re-assessment is only useful for doses of approximately 20 rads or greater.

Irradiation is not the only available means of increasing the dosimeter sensitivity. Wachter et al. (15) found sensitivity could be increased by 1) thermal treatment (such as the annealing procedure previously described) 2) optimizing the doping concentrations of Mg and Ti (for LiF TLDs), and 3) optimizing the concentration of hydroxyl ions (OH^-) in TLDs. The latter two methods of increasing sensitivity are not generally available since most TLD users buy their TLDs or powders in prefabricated form.

The storage of dose information in a TLD is dependent on the trapped electrons remaining in their respective traps until readout. The premature release of these electrons due to thermal or optical stimulation is known as fading. Fading may be greatly reduced by using the annealing procedure specified in Section 2.2 If oven annealing is not used, the TLD response will vary as a function of the storage time both before and after irradiation (16).

From the details given in this section it is apparent that the complete characterization of TL mechanisms in TLDs would involve a very complex model. In addition to the factors given above, a complete model should account for variations in response due to irradiation temperature, variations due to changes in LET and dependence of the response on the energy of the incident irradiation. One of the most complete models to date has been presented by Nakajima (17) and accounts for the three preceeding factors as well as supralinearity and sensitization.

3.0 Light Collection

The amount of light emitted by a TLD upon heating is directly proportional to the dose received. Therefore, the low end of the detectable dose range for TLDs is usually determined by the sensitivity and signal-to-noise ratio (SNR) obtainable with the light detection system. Several means of low level light detection are available - such as p-i-n photodiodes or photosil detectors - but the most sensitive known light detector at present in the visible and ultraviolet region is the photomultiplier tube or PMT.

3.1 Photomultiplier Tubes

A schematic of a typical PMT is shown in Fig. 3-1. The incident photons enter the evacuated enclosure through a window which has a semitransparent photocathode deposited on its inner surface. The interaction of the incident radiant energy with the electrons in the photocathode causes the emission of photoelectrons by the process of photoemission. The resulting photoelectrons are accelerated by an electric field toward the first dynode. The impact of the photoelectrons on the first dynode causes secondary emission, i.e., the production of secondary electrons which are accelerated by electric fields toward the second dynode. This process is repeated at the third dynode and continues down the dynode chain until the electrons leaving the last dynode are collected by the anode and become the PMT output.

The gain of the PMT is determined by the number of dynodes (or stages) and by the average number of secondary electrons emitted per incident electron. For instance, if there are 12 stages and 5 secondary

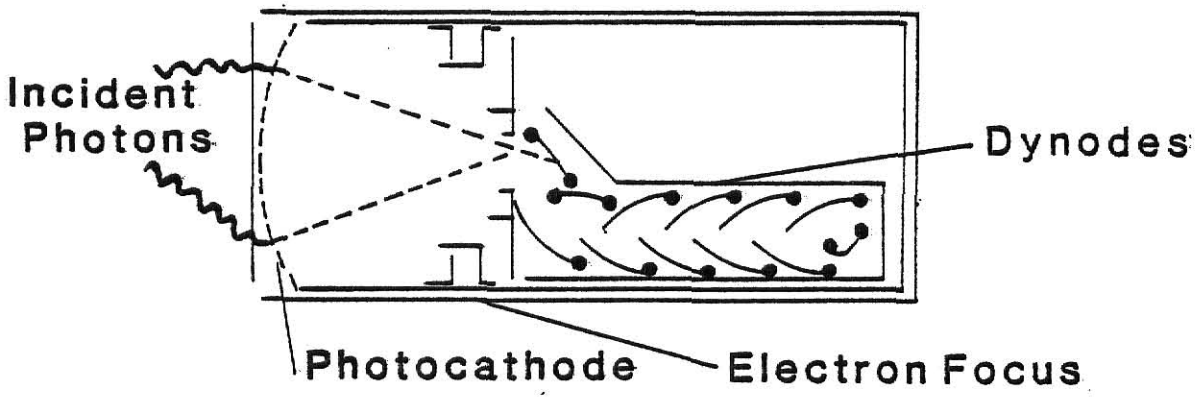

Fig. 3-1. Diagram of the basic components of a PMT (18).

electrons are emitted for every incident electron, the number of electrons collected at the anode corresponding to one photon at the photocathode will be 5^{12} or approximately 244 million.

The number of secondary electrons emitted per incident electron is not a constant but rather exhibits stochastic behavior. The statistical distribution most often used to model secondary emission is the Poisson. Prescott (19) has developed a more complex model based on the Polya distribution. This model has been accepted and used by several authors (e.g. (20)), but is still considered inadequate by others. Cafolla et al (21) have pointed out some shortcomings in the Prescott Model, the most important being the absence of a direct link with the basic mechanisms of secondary electron production. They present a Monte Carlo method for computing secondary emission which they claim overcomes these shortcomings.

The electric fields which are used to accelerate and focus the electrons are produced by maintaining the dynodes at appropriate electric potentials. These voltages are supplied by a single high voltage power supply through a resistive voltage divider network. It is important to select values of resistance and voltage which will keep the dynode potentials constant even when a pulse is traveling through the tube. Failure to do so may result in an unstable light collection system.

There are other potential sources of instability in a PMT, one of which is rate-dependent gain. Not only is the gain sometimes altered by a change in rate, but the gain change is also a function of the time after the rate change (22).

Another phenomenon affecting long term stability is known as fatigue. Fatigue is simply a gradual decrease of the PMT gain or sensitivity after extended use, especially at high current levels. Sensitivity changes that are a direct function of large currents imposed for great lengths of time are thought to be the result of erosion of cesium from the dynode surfaces and its subsequent deposition on other areas of the PMT (18). The erosion is caused by the intense electron bombardment corresponding to high output currents. This fatigue or sensitivity loss may be reversed when the PMT is not in use. It is postulated that this occurs because the cesium returns to the dynodes when the tube is not in operation. This return process may be accelerated by heating the tube as long as specified temperature ratings are not exceeded. PMTs with multi-alkali photocathodes also experience photocathode fatigue upon extended exposure to high room lighting. The mechanisms which cause this loss of sensitivity are not clearly understood but the damage is usually permanent.

3.2 Dark Current

A PMT with high voltage applied always produces an output signal, even in the absence of light. Because PMTs are more commonly used in the charge integration or current mode, the portion of the output which is not light-induced has been named dark current. The properties of dark current are not completely understood but it is believed to be the sum of several different components.

The dark component that is generally assumed to be dominant is caused by the thermionic emission of electrons from the photocathode.

Thermionic emission occurs because at temperatures above $0^{\circ}K$ some of the electrons will acquire sufficient energy to exceed the photocathode work function and escape the surface. These electrons cannot be differentiated from those induced by photons because both produce one or more electrons at the photocathode which are subsequently accelerated and multiplied through the dynode chain.

Because thermionic emission is a function of photocathode temperature it may be reduced by cooling the PMT. It has been shown (23) that when photocathode temperature is reduced from $30^{\circ}C$ to $-80^{\circ}C$, a reduction in dark current of more than a factor of 100 occurs. However, this does not result in a comparable improvement for SNR. As the tube is cooled the photocathode sensitivity also decreases. In addition, the tube's output current becomes more erratic. The decreased sensitivity and poorer statistics at low temperatures offset most of the advantage gained by reducing the thermionic emission. In fact, Harker (24) has shown that in some cases better results are obtained with an uncooled tube than with a cooled one.

Some authors (e.g. (25)) have suggested that the main component of dark current is due to the ionization of gas molecules by energetic electrons rather than thermionic emission. The positively charged ionized fragment is accelerated in the opposite direction as the electrons and thus will strike a dynode or the photocathode. These heavy ions will cause one or more electrons to be emitted when they strike the dynode or cathode surface. The size of the resulting pulses will vary widely depending on how many electrons were produced at impact and where in the PMT the pulses originate.

Because the ions are many times more massive than electrons,

the ion-induced pulses are correlated to the other pulses in the PMT but are delayed. This process is referred to as afterpulsing or positive ion feedback. If positive ion feedback is the main source of dark current, the decrease of dark current with decreasing temperature must be explained in terms of this phenomenon. Young (25) suggests that at lower temperatures more of the residual gas in the evacuated PMT is absorbed on solid surfaces which decreases the number of gas molecules available for ionization.

Another type of correlated afterpulsing is caused by an electron striking a metal surface and producing an X-ray. The X-ray may, in turn, cause another electron to be emitted from the photocathode just as if a photon had struck the photocathode.

A source of uncorrelated dark pulses is the presence of radioactive isotopes in the PMT structure itself. The largest and most widely reported effect of this type is that of beta particle production from the disintegration of ^{40}K in the glass envelope. A somewhat smaller but noticeable effect is the interaction of cosmic rays with the PMT. Although the cosmic ray pulse rate is only 1-2 cm^{-2}/min. (26), the individual pulses they induce may be hundreds of times larger than single electron pulses. Both ^{40}K disintegrations and cosmic rays can produce dark pulses either directly by interactions in the photocathode and dynodes or indirectly by causing Cerenkov light, scintillations, or phosphorescence in the glass envelope of the tube. The emitted light is, in general, a more important source of dark pulses than the direct interactions with cathode and dynodes (20).

Another source of dark current, in the charge integration mode, is ohmic leakage. Ohmic leakage results from the imperfect insulating properties of the glass stem, the supporting members of the base, and is always present but usually negligible. Contamination consisting of dirt, water vapor, or grease on the outside of the tube may also contribute to ohmic leakage (18). Because it is DC in nature, ohmic leakage has no effect on the output in the pulse counting mode.

One other type of noise which has been reported for PMTs is $\frac{1}{f}$ noise. $\frac{1}{f}$ noise is caused by resistance fluctuations in resistive circuit elements (27) and was named $\frac{1}{f}$ noise because its power spectrum exhibits approximately $\frac{1}{f}$ behavior. These reportings are few, however, and Young (25) suggest that $\frac{1}{f}$ noise is not generally important in PMTs.

3.3 Photon Counting vs. Analog Measurements

As stated previously, the output from a PMT may be counted as pulses or integrated and measured as current or accumulated charge. The advantages claimed for the pulse counting technique include: 1) discrimination against noise which does not originate at the photocathode - thereby increasing the system SNR, 2) digital processing of inherently discrete spectral information, 3) elimination of errors associated with data domain conversions, 4) sensitivity to very low light levels, 5) accurate long term integration, and 6) reduced sensitivity to $\frac{1}{f}$ noise, long term drift, voltage changes and temperature changes (28).

To illustrate how photon counting allows discrimination against noise not from the photocathode, Fig. 3-2 presents a typical PMT differential pulse height distribution (PHD).

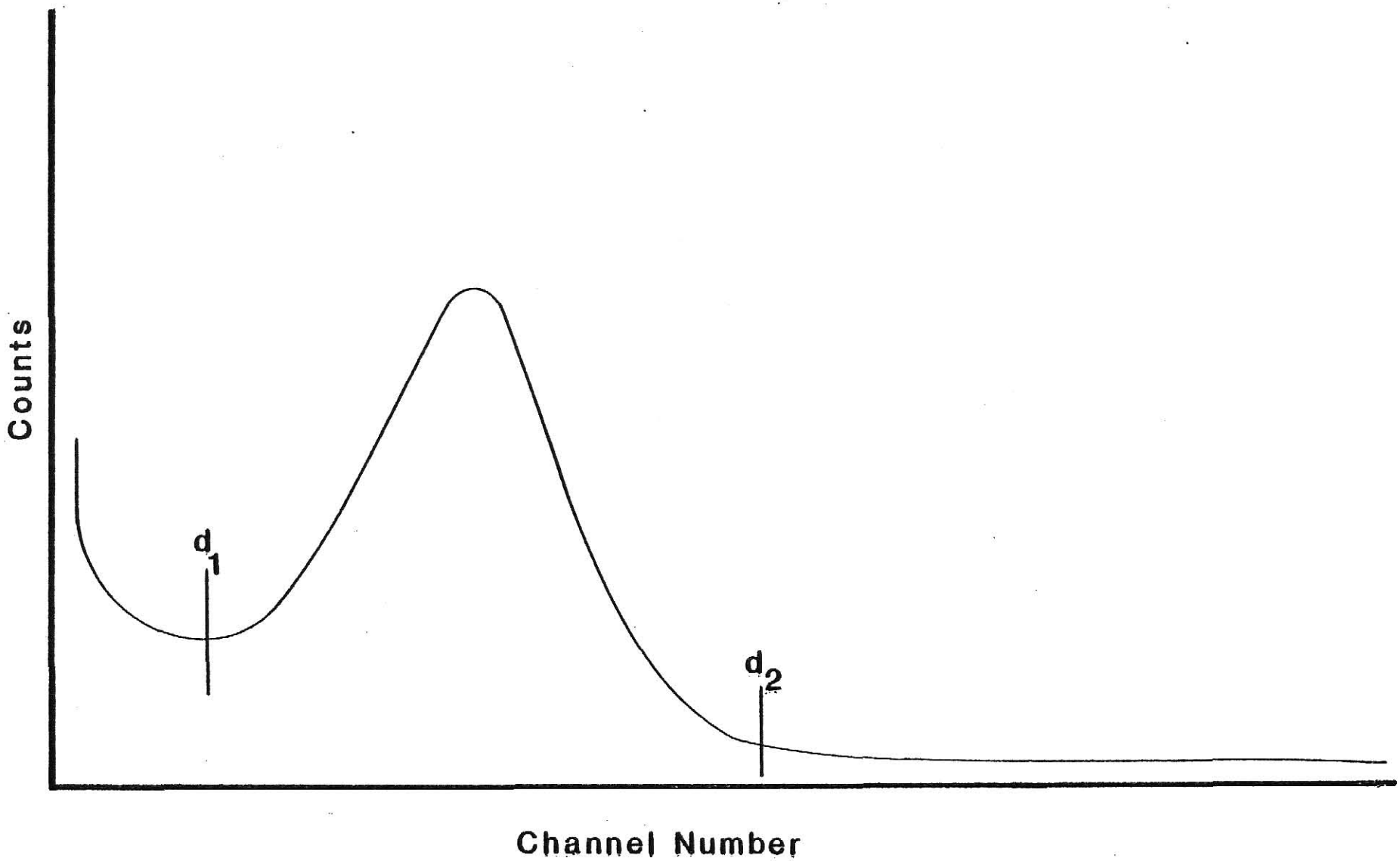

Fig. 3-2. A differential pulse height distribution for a PMT with lower and upper level discriminators d_1 and d_2, respectively.

A differential PHD is formed by plotting the number of pulses within a given incremental pulse height as a function of pulse height. Pulses falling between d_1 (lower level discriminator) and d_2 (upper level discriminator) are caused almost exclusively from electrons emitted at the photocathode. Pulses with height greater than d_2 are usually caused by cosmic rays or natural background from ^{40}K and other isotopes present in the tube materials. Pulses smaller than d_1 are usually caused by pulses which originate at one of the dynodes rather than at the photocathode. Since only pulses originating at the photocathode may be photon induced, it is advantageous to exclude all pulses with heights not between d_1 and d_2. Current mode measurements do not allow for discrimination by pulse height.

It is important to note that pulse height discrimination capability is of little value if the dark PHD has the same shape as the light or signal PHD because the SNR will be unaffected by the pulse height discrimination. Jones et al (29) have claimed that this is the case and that no improvement can be made by optimizing the discriminator levels.

Many authors have attempted to compare the SNRs obtainable using photon counting and analog measurement techniques to derive a ratio of photon counting to current mode sensitivity (20, 23, 25, 30-32 and others). These theoretical ratios range from one (31, 32) to three (23), with most falling between one and two. All theoretical ratios assume either Poisson or Polya statistical distributions and neglect such affects as cosmic ray and ^{40}K induced pulses. Therefore, experimental comparisons are necessary for an absolute determination of the SNR and sensitivity advantages of photon counting for a given system.

4.0 The Photon Counting System

A block diagram of the entire photon counting system is shown in Fig. 4-1. A brief overview of the readout process and the functions of the different components will be given first, followed by a more detailed description of the individual devices.

4.1 System Overview

The system is based around a Motorola M6800 microprocessor. A typical temperature profile of the microprocessor controlled readout cycle is depicted in Fig. 4-2. The ordinate represents the temperature of the planchet on which the TLD is heated; the abcissa represents time. The temperature output of the TLD readout unit is monitored by the microprocessor through one of the interface circuits.

Beginning at t_{open}; when the microprocessor senses that the planchet and the TLD from the previous cycle have cooled to T_{open} (approximately $100^{o}C$), a buzzer and an LED on the display signal the operator to open the drawer and replace the TLD. After the TLD has been replaced and the drawer shut, the microprocessor waits for the planchet to cool to T_{RS} ($60^{o}C$) at which time it turns on the heater in the readout unit and starts the multichannel analyzer (MCA). After a short and rapid preheat the temperature increases at a constant rate. When the microprocessor senses that T_1 has been reached the high speed counter is started. The counter remains on until the microprocessor shuts it off when the temperature exceeds T_2. After a short delay the heater in the readout unit is turned off and the cycle repeats when the planchet has cooled to the T_{open} temperature.

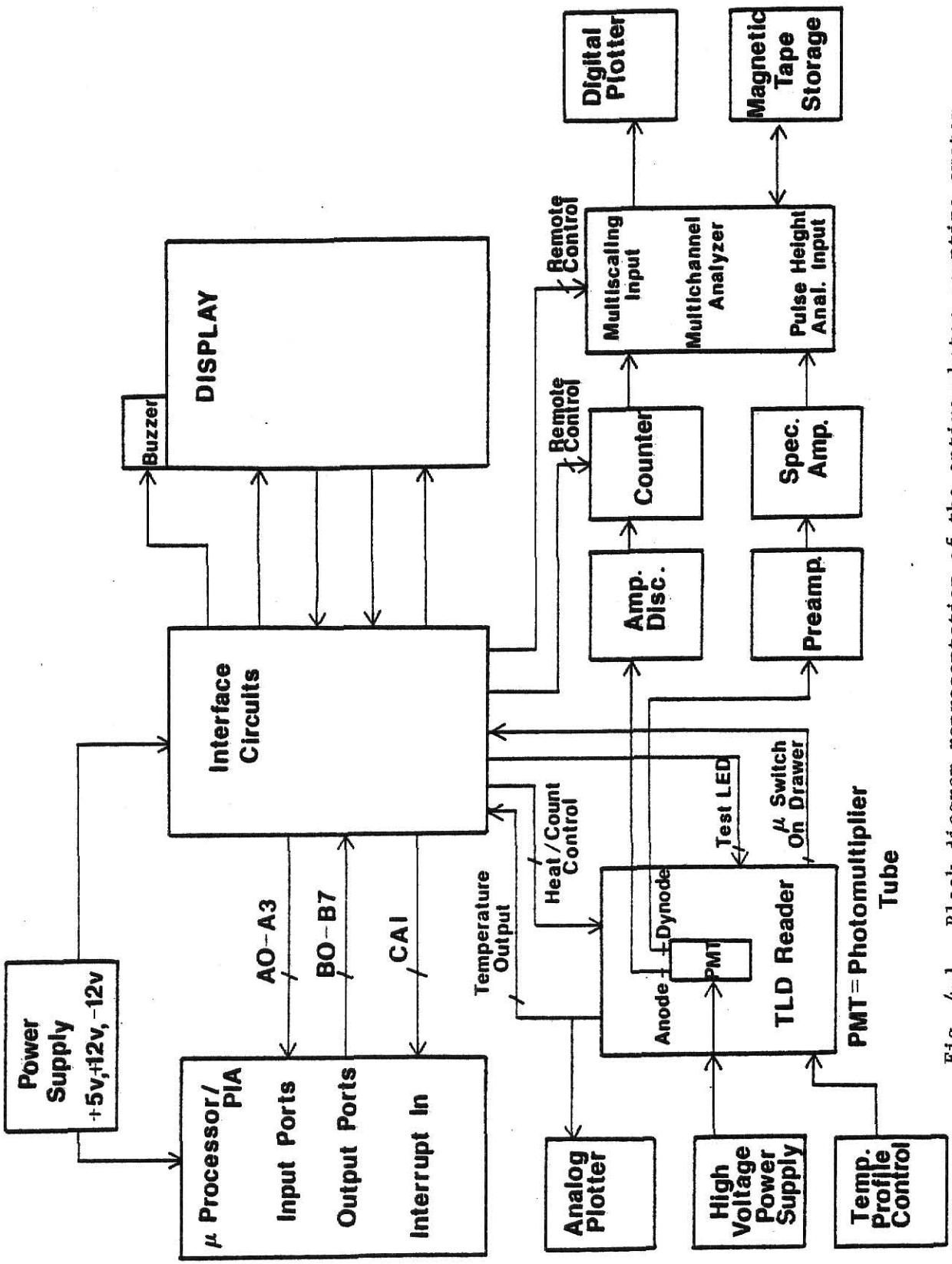

Fig. 4-1. Block diagram representation of the entire photon counting system.

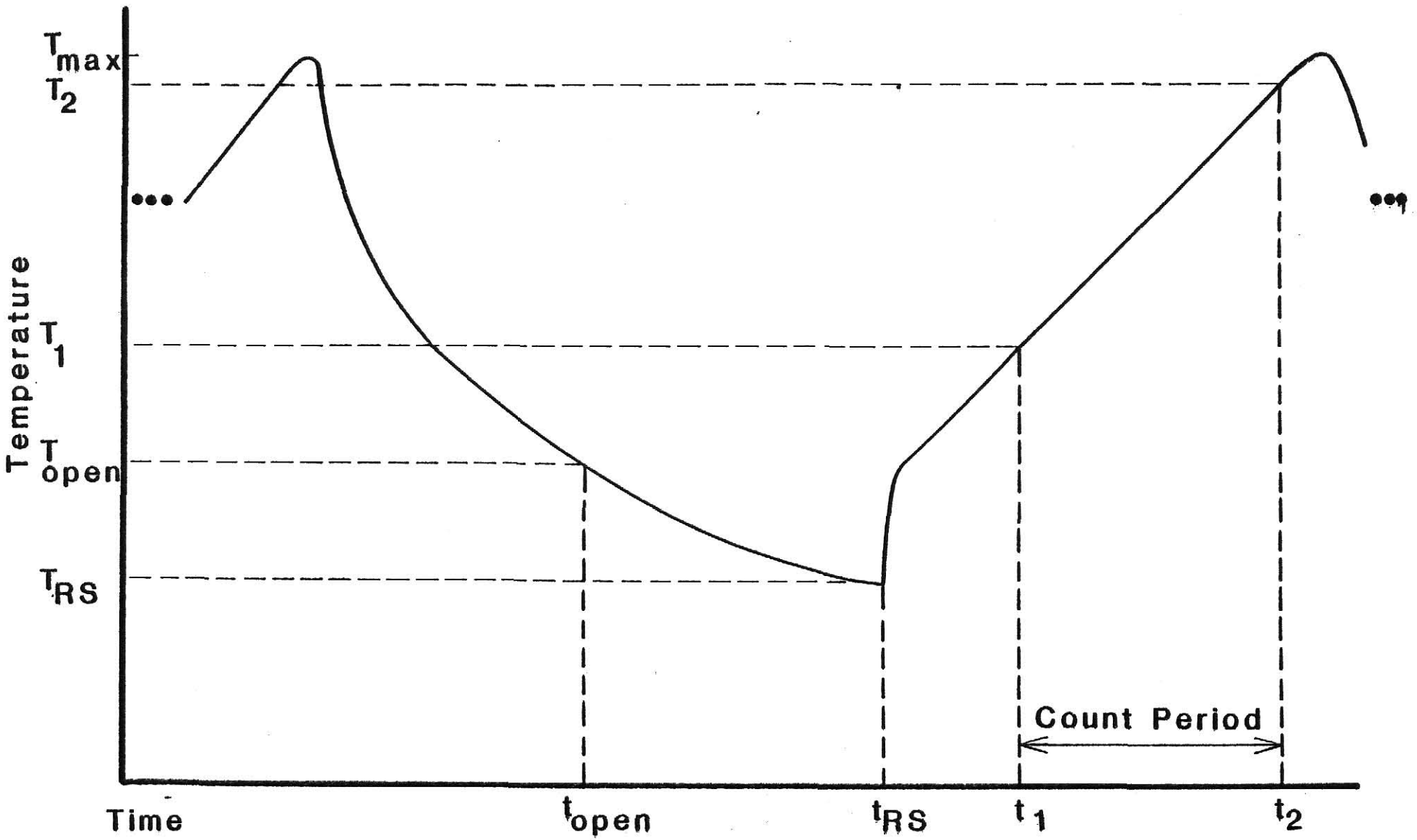

Fig. 4-2. A typical temperature profile of the microprocessor controlled readout cycle showing critical times (t) and temperatures (T).

After this description some of the advantages of a microprocessor controlled system are more apparent; 1) the cycle is more accurately reproduced by the microprocessor - especially the temperature triggered events, 2) because the software is easily changed the system is more versatile, and 3) it is more convenient for the operator who would find it difficult to start and stop the heater, counter, and MCA at the correct times as well as record data and replace TLDs.

4.2 The Microprocessor

The M6800 microprocessor was obtained as part of Motorola's M6800 D-2 Kit. This made the input/output and the programming much easier than if only the microprocessor integrated circuit (IC) itself had been used.

A basic form of the software program, PC CONTROL, was written and has been permanently recorded on an MC68708 Erasable Programmable Read Only Memory (EPROM). However, for most of the experimental work the program was transferred to the microprocessor's Random Access Memory (RAM) where it could be easily modified when necessary. A short program for transferring the main program from ROM to RAM is provided in Appendix A. Also in the appendices are a flow chart (Appendix B), program listing (Appendix C), and a user's manual (Appendix D) to aid in system operation and program modification.

4.3 Interface Circuits

The simple interface circuits required for the system are shown in Figs. 4-3, 4-4, and 4-5. Unfortunately, not all the system components

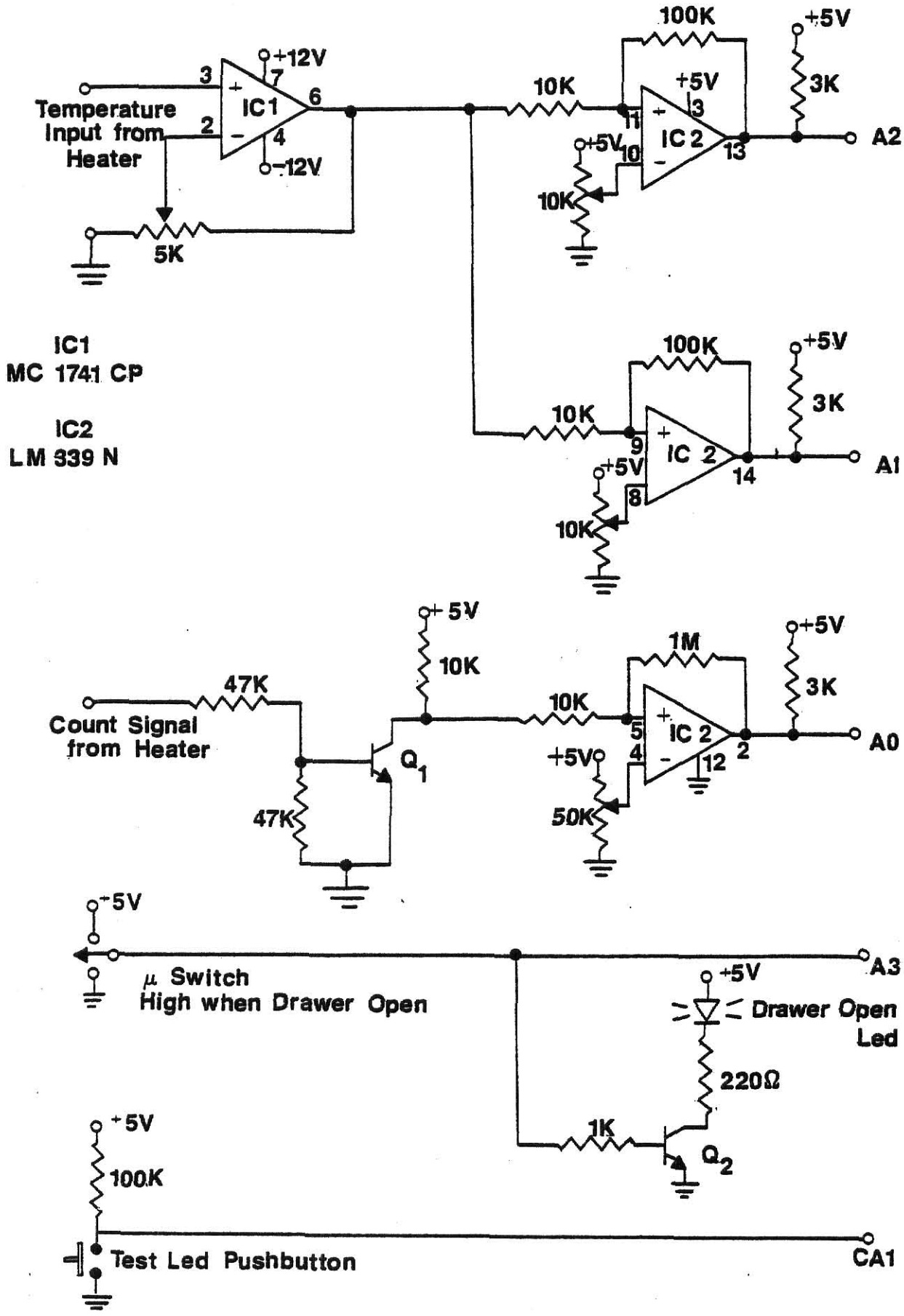

Fig. 4-3. Interface circuits used for the inputs to microprocessor port A.

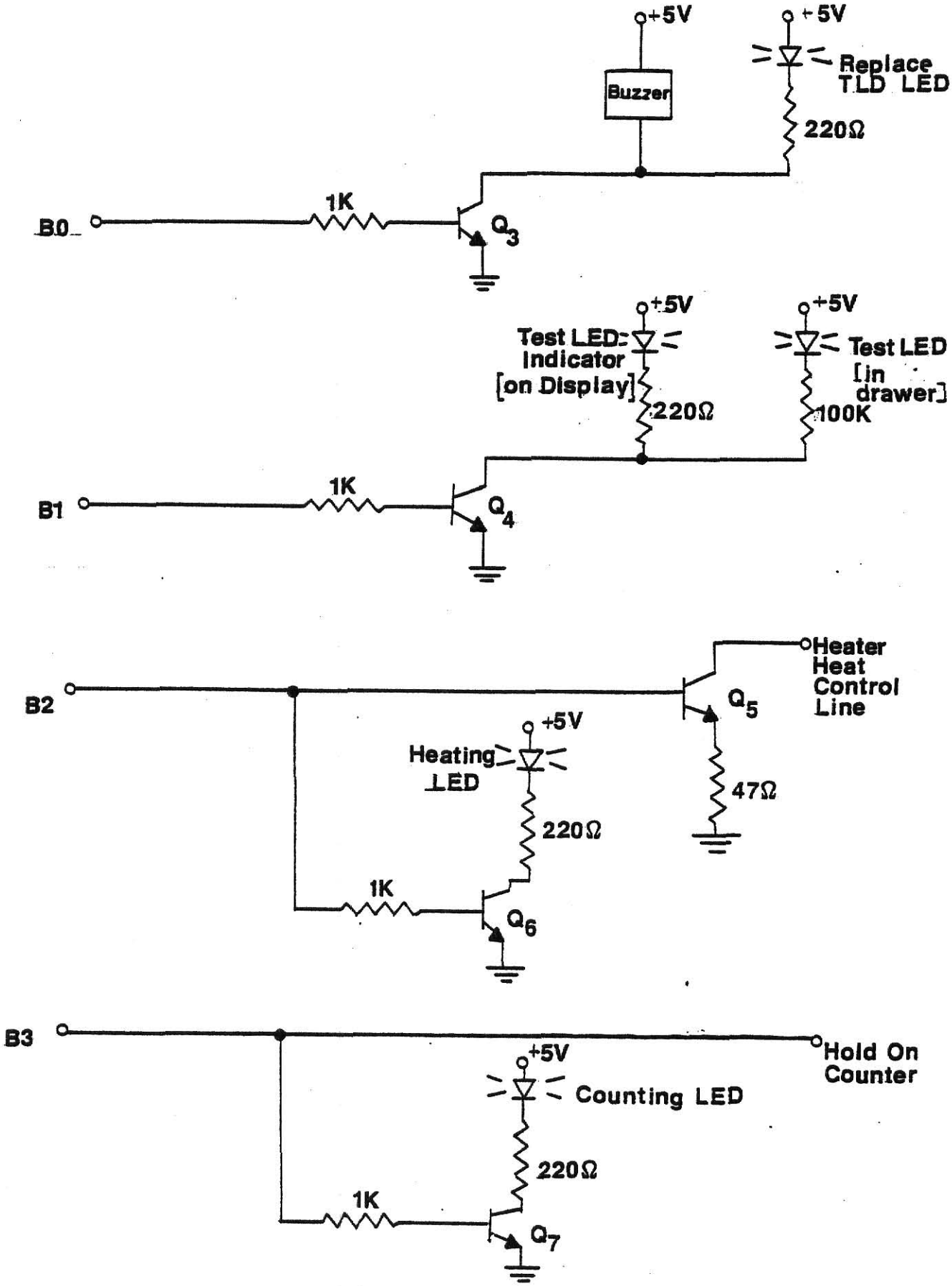

Fig. 4-4. Interface circuits used for the outputs from microprocessor port B, bits B0-B3.

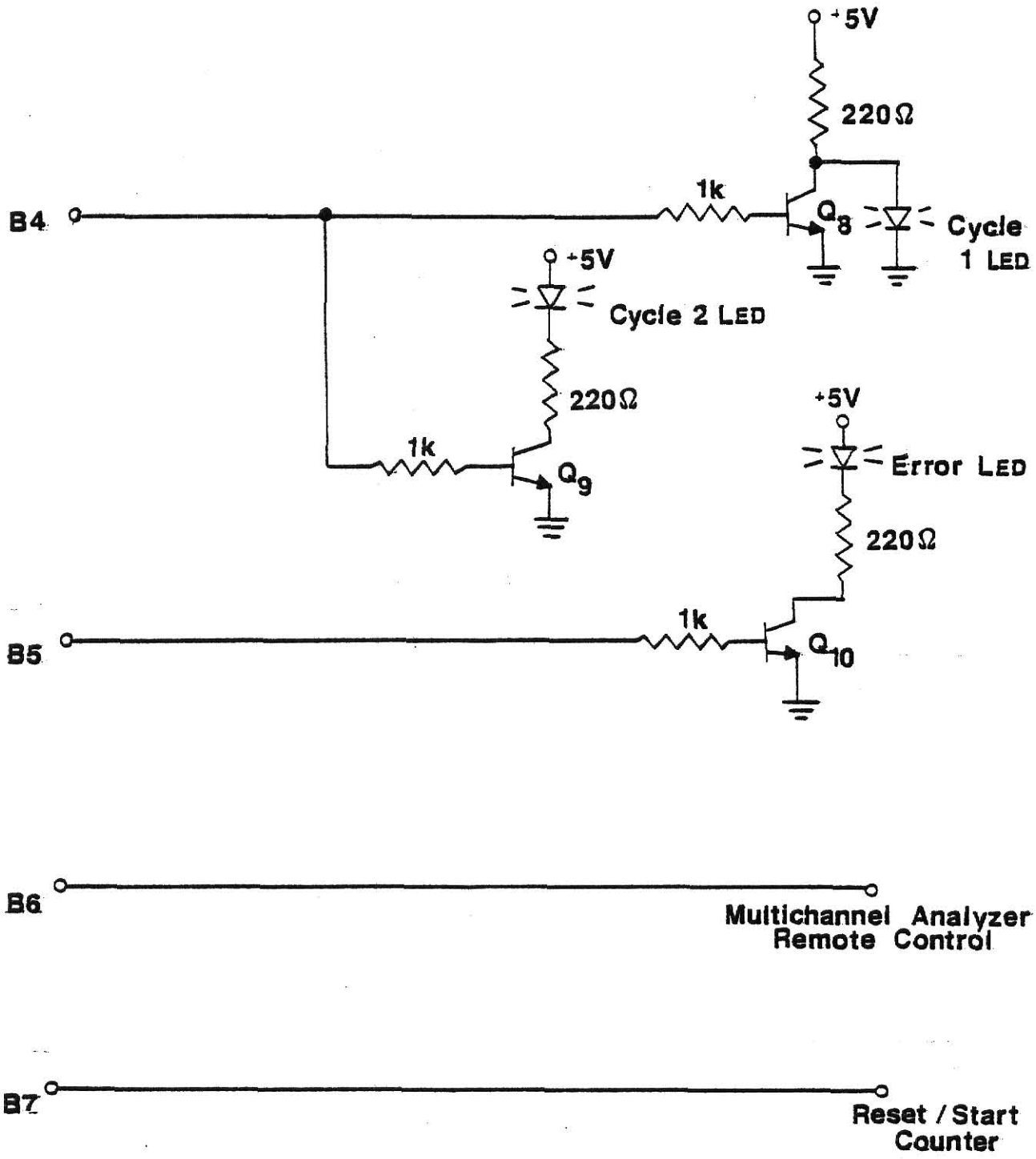

Fig. 4-5. Interface circuits used for the outputs from microprocessor port B, bits B4-B7.

could be controlled by TTL logic level signals so transistor interfaces were required in addition to the transistor drivers used for the display.

The temperature sensing circuit shown in the top portion of Fig. 4-3 consists of an adjustable gain amplifier followed by two comparators in parallel. The comparator circuits, which employ hysteresis to reduce instability, change output states when the + input changes polarity with respect to the - input which is set via a potentiometer to correspond to T_1 or T_2. The display is provided to indicate to the operator: which portion of the cycle is being executed, when operator action is required, that the system is functioning correctly, and if an operator error has been made by not replacing the old TLD and shutting the drawer before the planchet cools to T_{RS}.

4.4 Readout Unit

The readout unit is a modified Harshaw 2000A Thermoluminescence Detector. The original PMT and its housing were removed and replaced with an RCA 8850 PMT in an Ortec 9201 PMT Housing/Voltage Divider. A lens and mirror which preceeded the PMT were also removed because it has been reported that fluorescence in the lens causes an increase in the dark signal by a factor of five (9). This also made it possible to place the PMT much closer to the planchet which improved the light collection efficiency.

This particular 8850 PMT was selected by RCA for critical applications because of its low noise characteristics. The 8850 has a high quantum efficiency bialkali photocathode, and an extremely high

gain gallium-phosphide first dynode which gives good pulse resolution at the output. The spectral response of the 8850 is shown in Fig. 4-6 along with the emission spectra for LiF TLDs, CaF_2: Mn TLDs, and a green HP 5082-4984 LED used as a light source. The spectral characteristics of the TLDs and the PMT match relatively well but a blue LED light source (if available) would be more desireable.

The LED was mounted in the back of the drawer containing the planchet in place of the ^{14}C activated NaI(Tl) light source that came with the unit. The LED was used in place of the light source because its intensity was adjustable and hopefully more stable. Nollman et al (33) pointed out a 5% inconstancy in the light source provided with their TLD readout unit. When the drawer is opened to change TLDs, the LED is under the PMT so the microprocessor may perform a stability check by turning the LED and the counter on for a short test. An alternative would be to connect the LED to a precision regulated picoammeter source. This would make the light intensity adjustable over the full range of the photon counter for optimization, pulse pile up measurements, and other related tests.

The Harshaw readout unit was originally equipped with an infrared filter which pivots down between the planchet and the PMT when the drawer is inserted and springs up out of the way when the drawer is pulled out. One of the goals of this research was to determine if a neutral density optical filter could be used to reduce the light intensity at the PMT and thus extend the upper limit of the dose range for which the system is useful. To make available the option of inserting a neutral density filter it was necessary to redesign the filter holder.

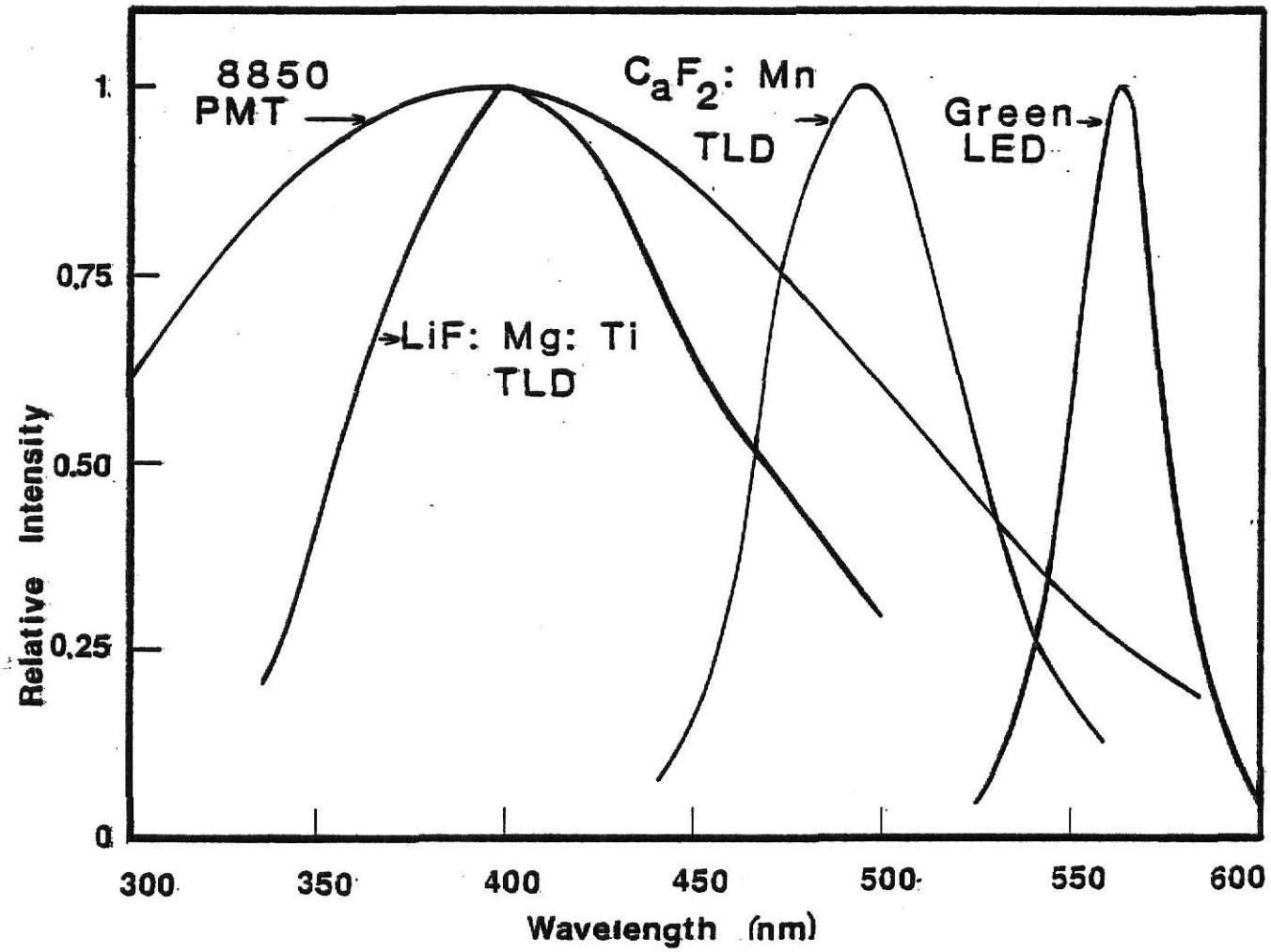

Fig. 4-6. Comparison of the RCA 8850 PMT spectral response with the emission spectra for LiF TLDs, CaF_2:Mn TLDs, and a green HP 5082-4984 LED.

The new holder, shown in Fig. 4-7, consists of a triple-tiered ring which fits into a square aluminum frame and is held by a set screw. The two inner diameters of the ring are such that the infrared filter and the neutral density filter may be inserted, one on top of the other, or the neutral density filter may be removed and replaced with the spacer ring.

The Harshaw 2000A readout unit is designed to operate in conjunction with the Harshaw 2000B Integrating Picoammeter which contains the power supplies for both units. Since the 2000B was not needed for photon counting, a separate power supply to provide ±15 V DC and 110 V AC to the readout unit was added to the system. The high voltage power supply which supplies the biasing voltages for the PMT is a Canberra Model 3002.

In the temperature profile, shown in Fig. 4-2, there are three adjustable parameters controlled by potentiometers on the Harshaw readout unit: the preheat temperature, the rate of temperature change, and the maximum temperature the planchet will be allowed to reach. It is often desirable to have different temperature profiles available for different types of TLDs. To make the change from one profile to another more convenient, a temperature profile controller was added to the system. The controller allows three different profiles to be preset on three sets of potentiometers, one of which may then be selected by simply adjusting a single three position switch.

It was pointed out in Chapter 3 that cooling the PMT may not improve the SNR because of the decreased photocathode sensitivity and high variance in the dark signal. Tube cooling may also cause moisture

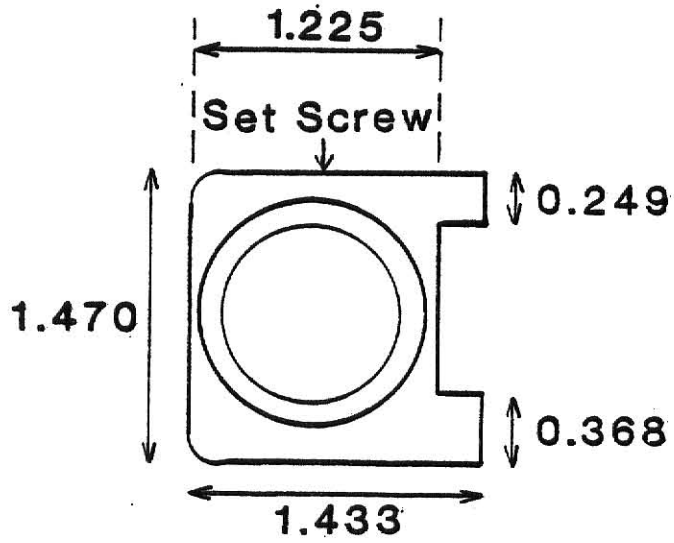

(a)

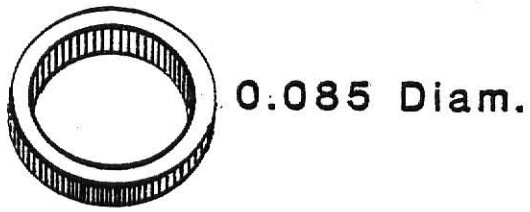

(b)

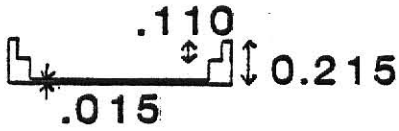

Cut Away Section

Diameter
D_1=1.100
D_2=0.988
D_3=0.858
D_4=0.788

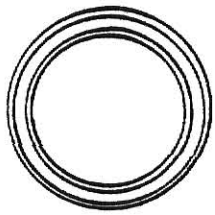

Top View

(c)

Fig. 4-7. Redesigned filter holder: a) aluminum frame, b) spacer ring, c) cut away and top view of tiered ring (dimensions in inches).

condensation on the surface of the PMT window (8) which interferes with efficient light collection. But it is desireable to maintain the PMT at a constant temperature to improve the system's stability. For this reason a thermoelectric cooler was attached to the tube housing to keep the PMT at a constant temperature several degrees below room temperature. The thermoelectric cooler also serves as a temperature reference for the thermocouple circuit which detects the planchet temperature.

It was mentioned in Chapter 2 that heating the TLD in an inert atmosphere helps reduce chemiluminescence. Some authors (e.g. (7)) have reported the use of helium to provide the inert atmosphere, but helium is a poor choice because it permeates through the glass envelope of the PMT causing an increase in noise and eventually filling the tube sufficiently to make it inoperative (18). Therefore, a continuous flow of dry nitrogen was used to fill the drawer chamber before each readout.

4.5 Data Collectors

The pulses leaving the PMT are collected as data by the high speed counter and by the MCA. The counter is a Model 1109 Photon Counter made by Princeton Applied Research (PAR). Pulses recorded by the counter first pass through its companion Amplifier-Discriminator Model 1121. The remote preamplifier unit of the 1121 is connected to the PMT anode output by a six inch coaxial cable to minimize the noise added during transmission. The discriminator unit provides the capability of using an upper and lower level discriminator and of engaging a 100 MHz divide-by-ten prescaler.

The Canberra Series 80 MCA may be used to collect data in two different modes. In the multiscaling mode, logic pulses from the counter

are fed to the multiscaling input to produce a digital glow curve. In the pulse height analysis mode (PHA), pulses are collected from the PMT's last dynode by an Ortec 113 preamplifier in series with an Ortec 451 Spectroscopy Amplifier. These pulses are then passed to the ADC (Analog-to-Digital Convertor) input to produce a differential pulse height distribution like the one shown in Fig. 3-2. Pulse height distributions or glow curves collected with the analyzer may be plotted on the digital plotter or stored on magnetic tape. Because the MCA may be programmed and remotely controlled, it is possible to record glow curves for a set of TLDs without the need for reinitializing between each cycle. Magnetic tape storage also makes it possible to read the data into a large computer facility for data analysis.

4.6 Equipment Problems

Over the five months that the system was used for this research it failed only twice (all instruments were left on continuously). Both failures occurred overnight and simply required the replacement of the fuse in the Harshaw readout unit. There were three other problems which did not incapacitate the system but should be mentioned.

4.6.1 Oscillations on the Harshaw Integrate Signal

The version of the Harshaw 2000A used in this research came equipped with the two comparators required to sense T_1 and T_2, and with the calibrated potentiometers to control them. A signal labeled "Integrate", which corresponds to T_1 and T_2, is available from the unit. Integrate is high when the cycle starts, low when the planchet temperature is between T_1 and T_2 and then returns high when the temperature

exceeds T_2. It was decided to use the "Integrate" signal and take advantage of the calibrated potentiometers rather than design two more comparator circuits. The problem arises from the lack of hysteresis on the 2000A comparator circuits. Without hysteresis the comparators oscillate severely for several seconds when the planchet temperature approaches one of the switching temperatures, T_1 or T_2. This means that after T_1, a four second software delay is required before the microprocessor may begin checking to see if T_2 has been reached. Depending on the heating rate this limits the minimum width of the temperature window to approximately 50°C.

Checking an identical 2000A in current mode operation with the 2000B Picoammeter revealed that approximately 50°C was the minimum temperature window obtainable in regular current operation also. Because the emitters of the comparators were used as outputs in the Harshaw 2000A circuits rather than the collectors, there was no simple way to add effective hysteresis to the circuit. The temperature windows required for this work turned out to be greater than 50°C so this was not really a problem, but in cases where narrow windows may be required it would be advisable to add two external comparators with hysteresis rather than use those provided.

4.6.2 The Amplifier-Discriminator and False Counts

Unstabilized comparators also present a problem in the 1121 Amplifier-Discriminator module. In these circuits two high-speed comparators with ECL outputs are used as the pulse height discriminators. Hysteresis is intentionally omitted to make their response as fast as

possible. Without stabilization these comparators are prone to oscillations when the discriminator bias voltages are adjusted to a level near zero volts, the DC voltage level on the signal input to the comparator. A bit of experimenting showed that operating the discriminator levels above the 2 point on the 0 to 10 discriminator scale adequately resolved the problem.

It was also found that a fixed frequency periodic pulse train could be counted at up to twice its true rate by adjusting the pulse heights to a value very near that of the discriminator reference voltage. The operator is not warned about these problems in the Princeton Applied Research Instrument Manuals (34,35), but they are discussed by two authors who built their own high speed discriminator-counters.

Darland et al. (28) and Borders et al (36) used the same IC comparator as PAR in their discriminators. It appears that this problem with false counts from the comparator (which Borders calls "False Alarm Rate") is inevitable with present IC technology. It is worth noting that both authors were able to build their relatively simple counters for less than $150. Darland's design does not take advantage of the capabilities of ECL circuits such as transmission line drive capability and high speed counting. Border's circuit, on the other hand, reportedly offers performance which exceeds the capabilities of the PAR system used here.

4.6.3 LED Instability and Nonlinearity

Although the LED light source may be more stable than the ^{14}C activated source, it has too large a temperature coefficient to be a reliable long term reference. A method of improving a system's stability

with an LED light source has been presented by Reiter and Stengl (37,38).

They used a p-i-n photodiode in a feedback circuit to stabilize the light output of the LED. This greatly increases the system's immunity to temperature changes because they report a temperature coefficient of $-4x10^{-4}/^{o}C$ for the p-i-n photodiode compared to $-3.5x10^{-3}/^{o}C$ for the LED. The resulting temperature coefficient for the stabilized LED was $2x10^{-4}/^{o}C$, more than a factor of ten improvement.

It would also be convenient if the LED intensity increased linearly with forward current. This would make the LED ideal for performing linearty checks on the light collection system using a precision picoammeter source. Unfortunately, the LED response is more nearly exponential with respect to current so LEDs are not well suited for simple linearty checks.

5.0 Optimization of Operating Parameters

Once a photon counting system has been assembled and is operating correctly, the user must decide what values of the adjustable operating parameters (discriminators, high voltage (HV), and heating rate) will give the best results. The goal in optimizing this system has been to maximize the accuracy and sensitivity of the photon counter (i.e. its ability to reliably measure the extremely small light signals corresponding to small doses) without sacrificing system stability and reliability. The procedures used to select the optimal operating conditions, as well as the resulting value of each optimized parameter, are described in this chapter.

5.1 Signal-to-Noise Ratio

An explanation of how pulse-height discrimination may improve signal-to-noise ratio (SNR) was given in Section 3.3. It was pointed out that if the dark DPHD and the light DPHD were of the same shape, no advantage from the use of discriminators could be realized. Figure 5-1 presents a comparison of a light and dark DPHD for this system. Inspection of the figure suggests that the DPHDs are significantly different and that a lower level discriminator (LLD) may be very useful in improving the SNR.

Several criteria have been reported in the literature for selecting the best discriminator levels. All these criteria have been labeled SNR by the authors but only one is a true SNR. Part of the problem arises from the fact that a PMT is a <u>quantum</u> detector. Signal-to-noise ratios are most often used in analyzing energy detectors or systems where SNR

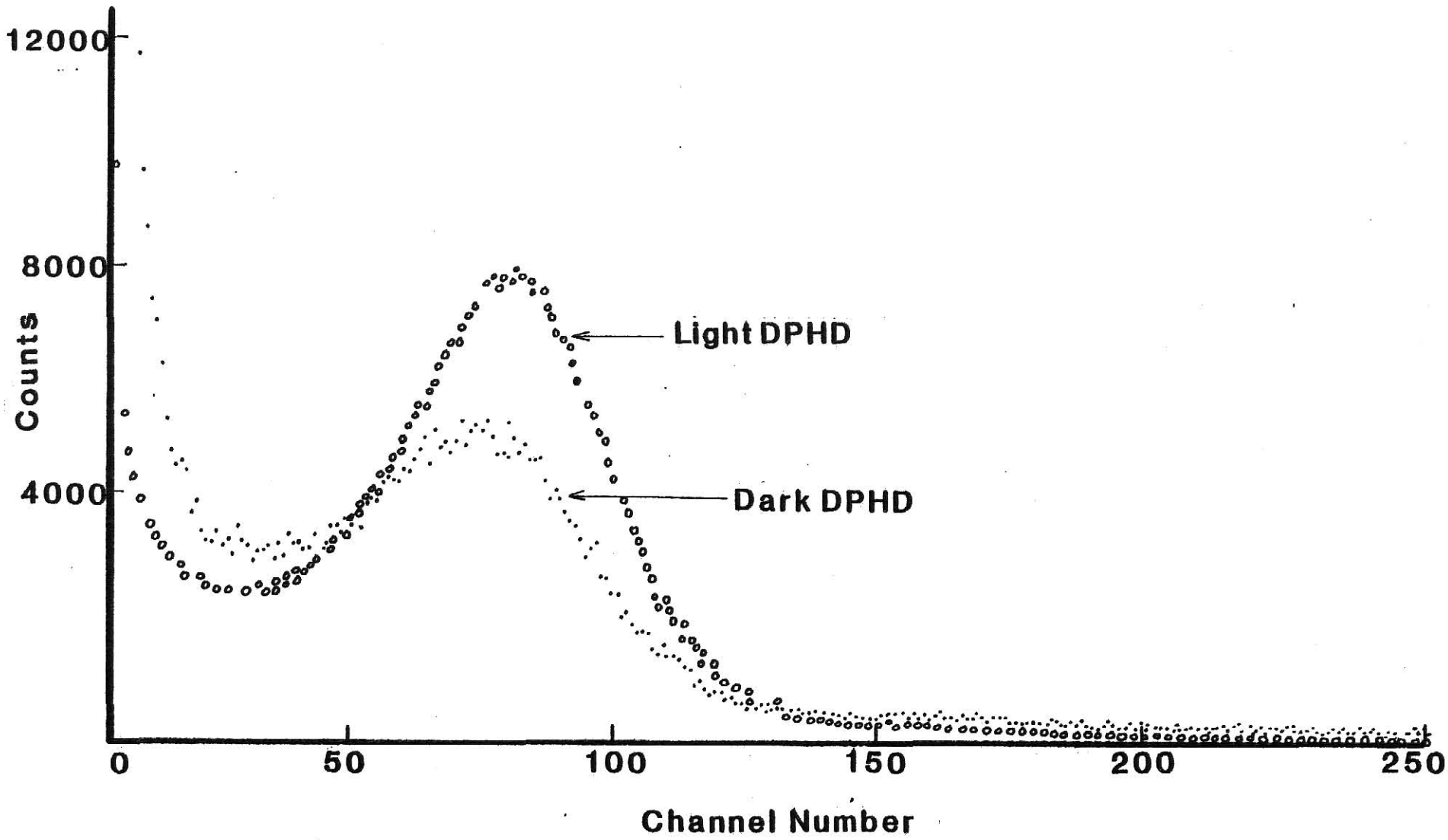

Fig. 5-1. Comparison of a light and dark differential pulse height distribution with HV=2200 V and an LED drive current of 1.00 μA. The dark DPHD has been increased in magnitude by a factor of eight.

is simply the ratio of signal output power to noise output power. However, this notion is not applicable to quantum detectors such as PMTs.

In order to examine SNR in more detail, the following quantities are defined:

T ≡ the total number of counts recorded when a light source is present. If more than one measurement is made T represents the average of these values.

D ≡ the number of counts recorded when no light source is present. If more than one measurement is made D represents the average of these values. Note: T and D are actually integral PHDs because they may be obtained by integrating a DPHD.

S ≡ T-D, the number of counts corresponding to the light signal.

s_T ≡ the standard deviation of T.

s_S ≡ the standard deviation of S.

s_D ≡ the standard deviation of D.

To distinguish the true SNR from the erroneous criteria reported in the literature, the latter will be referred to as performance ratios (of which SNR is a special case). Using the terms defined above, several examples of the performance ratios found in the literature may be expressed as follows: T/D (8), T/s_D, T/s_T (39), and S/s_S (32).

When making low dose measurements where the values of T and D are of the same order of magnitude, the largest source of inaccuracy or noise is the statistical variation in both T and D, even under constant operating conditions. Any performance ratio used to optimize the discriminator levels should include the effects of the noise (standard deviation) in the total signal and the noise (standard deviation) in the

dark signal. The correct expression for SNR which does include these terms was first presented by Morton (40). The equation Morton presented,

$$SNR = \frac{T - D}{(s_T^2 + s_D^2)^{\frac{1}{2}}} \tag{5-1}$$

has more recently been affirmed and used by others (41,42).

Most authors who use Eq. (5-1) assume that T and D may be described by random variables with Poisson distributions. This assumption allows the following substitutions to be made in Eq. (5-1): $s_T^2 = T$ and $s_D^2 = D$. Although virtually all authors make the assumption that T and D can be described by Poisson distributions, several have reported a variance (s_D^2) in the dark signal which is greater than that predicted by Poisson statistics (23, 31). Therefore, a more accurate measurement of SNR would use experimentally determined values of s_T^2 and s_D^2. To indicate when the Poisson assumptions have been made, two forms of Eq. (5-1) are used in the following analysis. The first, given the symbol S/N, utilizes the Poisson assumptions. The second, given the symbol S/N EX, makes use of experimentally determined values of s_T^2 and s_D^2. These two forms are presented below:

$$S/N = \frac{T - D}{(T+D)^{\frac{1}{2}}} \tag{5-2}$$

$$S/N\ EX = \frac{T - D}{(s_T^2 + s_D^2)^{\frac{1}{2}}} \quad . \tag{5-3}$$

5.2 Measurement of Performance Ratios

Because erroneous performance ratios have been used in the literature for selecting optimal discriminator levels, it was pertinent to

investigate the difference in the resulting discriminator levels obtained when using the true SNR compared to the other performance ratios. In order to make this comparison DPHDs were collected as follows: Pulses from the last dynode of the PMT were transmitted through a preamplifier and a spectroscopy amplifier to the PHA input of the MCA as shown in Fig. 4-1. After allowing the system to stabilize for several hours the MCA was programmed to accumulate a dark DPHD for 1000 seconds (live time), store the resulting data on magnetic tape, and accumulate again until ten dark DPHDs had been collected and stored. The same procedure was then repeated with the LED light source on to obtain ten light DPHDs on tape. (It would have been very time consuming to collect 1000 second DPHDs by reading out TLDs. It was found that the LED light source could be used for these tests instead of TLDs because they have nearly identical DPHDs, as shown in Fig. 5-2.) The tape was then transferred to the KSU computing facility to make the data available for computer analysis.

The computer program used to analyze the data was OPTPC. This program first reads the data from the tape into an array. Then, starting at MCA channel number 255 (which corresponds to the largest pulse height) and working towards channel number 0, the area (number of counts) under each DPHD is calculated between the current channel (Lower Level Discriminator, LLD) and channel 255. The ten values obtained for the light DPHDs are averaged as are the ten values from the dark DPHDs. These means and their associated variances, s_T^2 and s_D^2, are used to calculate S/N, S/N EX, and the following performance ratios: $\frac{T-D}{D}$, $\frac{T}{D}$, $\frac{T}{D^{\frac{1}{2}}}$, $\frac{T}{s_D}$, $\frac{T-D}{D^{\frac{1}{2}}}$, and $\frac{T-D}{s_D}$. Several of these ratios are identical to those

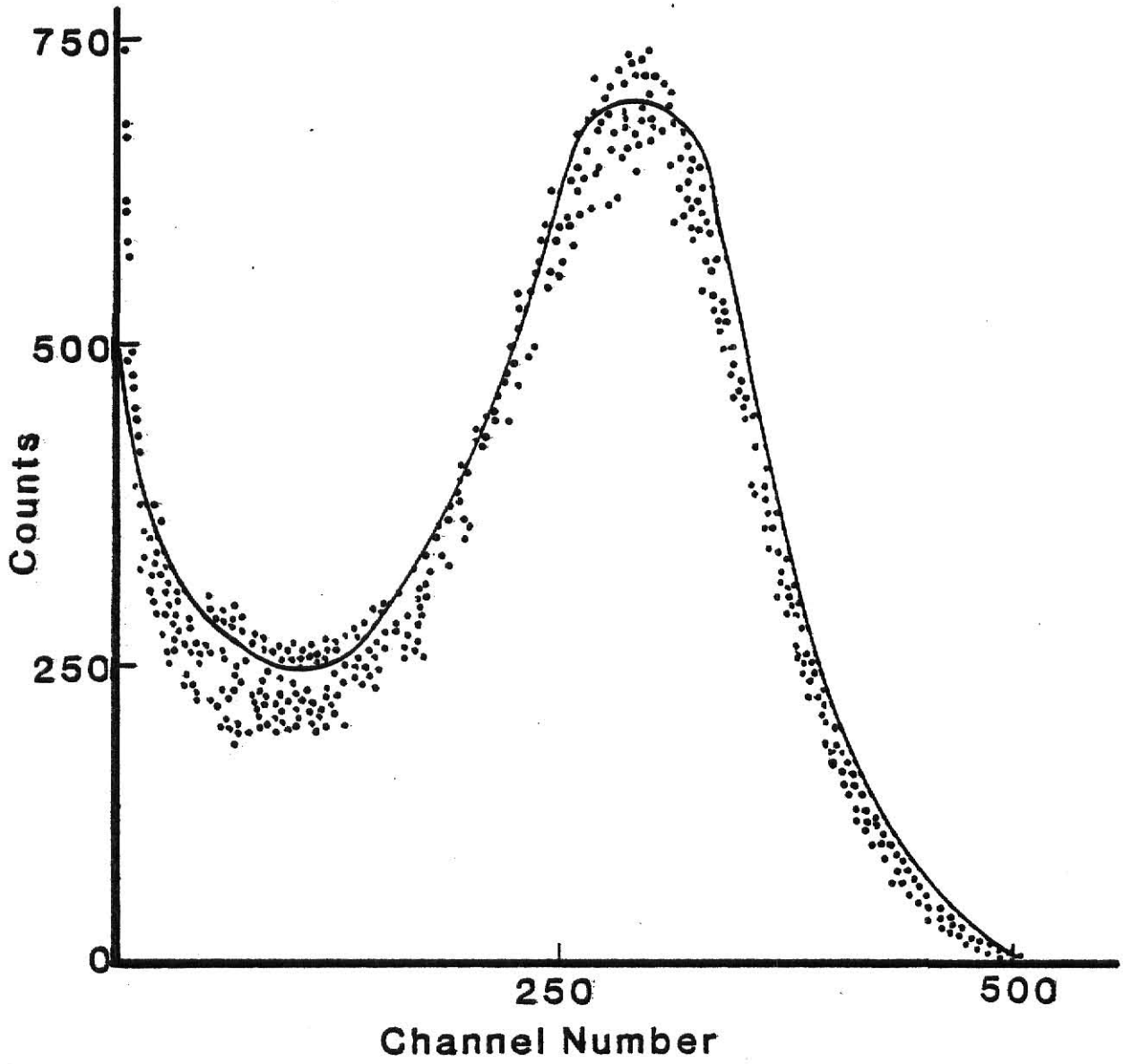

Fig. 5-2. Comparison of the differential pulse height distributions for the green HP 5082-4984 LED light source (dots) and for LiF (TLD-700) TLDs (solid line).

taken from the literature (see Section 5.1), the rest are similar forms used to observe the effect of making changes in the equations such as using (T-D) instead of T. These data are tabulated as a function of channel number and the program indicates the LLD setting which gives the maximum value of each ratio. Then the program begins at the optimum lower level selected for each ratio and calculates the same ratios as a function of Upper Level Discriminator (ULD). This results in a ULD and an LLD which give the maximum value of each ratio indicated above. To check the validity of Poisson assumptions, a table of s_D, $D^{\frac{1}{2}}$, s_T, and $T^{\frac{1}{2}}$ as functions of channel number is also provided. A listing of the program OPTPC is given in Appendix E.

5.3 *Results of Performance Ratio Tests*

The comparison of the performance ratios was performed over a range of HVs from 1800 to 2500 V. The LED light source used for collecting the light DPHD was driven by a 1.00 μA current which produced a counting rate approximately five times greater than that for the dark DPHD. Tests were also performed with light intensities approximately 100 to 1000 times greater which confirmed that the optimum discriminator levels selected were not dependent on count rate.

A comparison of a light and dark DPHD obtained with HV = 2200 V and an LED current of 1.00 μA was shown in Fig. 5-1. The dark DPHD has been increased in magnitude by a factor of eight to make the distributions easier to compare. A comparison of S/N and S/N EX for the same HV and LED current is shown in Fig. 5-3. From this figure it can be seen that the optimum value of S/N occurs at approximately channel number seven while the optimum value of S/N EX occurs near channel number

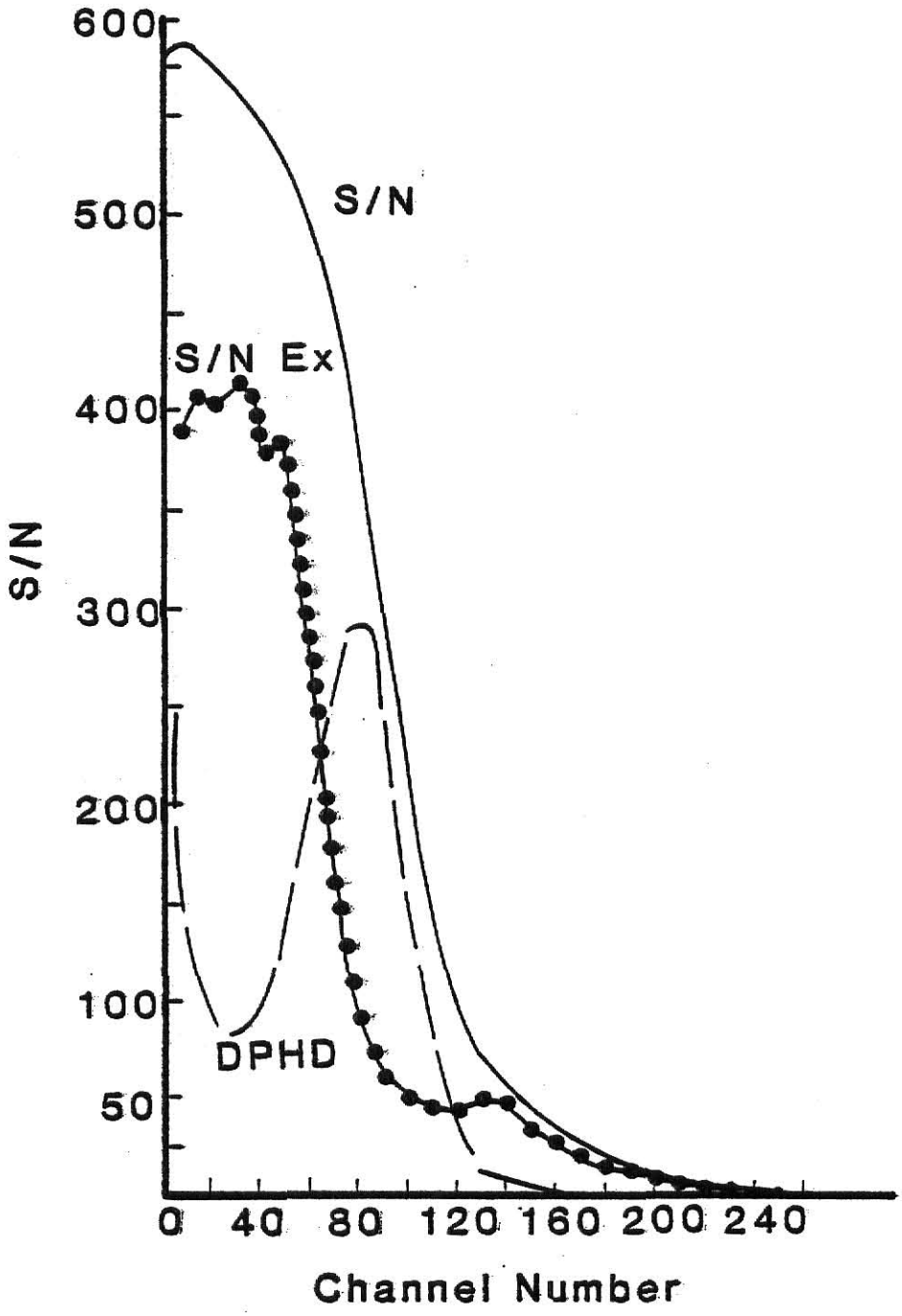

Fig. 5-3. Comparison of S/N and S/N EX as functions of LLD (channel number) for HV=2200 V and an LED drive current of 1.00 μA.

33 which corresponds to the valley on the DPHD. These results are significantly different and support the assertion that variance should be measured experimentally rather than assuming it is given by the square root of the mean.

The light DPHD, shown in Fig. 5-4, illustrates the optimum values of the LLD and ULD for the various performance ratios given in Section 5.2. Obviously it is important to select the correct SNR as they give widely varying results. Note that the correct form, S/N EX, indicates an optimum LLD in the valley of the DPHD and an optimum ULD at the base of the peak on the opposite side. These results are intuitively appealing and are identical to the instructions given in the PAR amplifier-discriminator manual for selecting upper and lower level discriminators(34). The manual, however, gives no further explanation or justification as to why one should use this procedure. Another factor which makes the S/N EX results appealing is that these optimum discriminator settings correspond to the discriminator levels which give the best system stability as will be explained in Section 5.4.

A comparison of the Poisson and experimental standard deviations for the dark DPHD is shown in Fig. 5-5 as a function of LLD. The experimental standard deviation is significantly greater as was expected. The Poisson and experimental standard deviations for the light DPHD are shown in Fig. 5-6. The experimental standard deviation is not only larger than the Poisson, it also exhibits a large peak in the same region as the peak of the light DPHD. This result has not been reported or explained in any of the available literature. Therefore, the following is offered as a possible explanation.

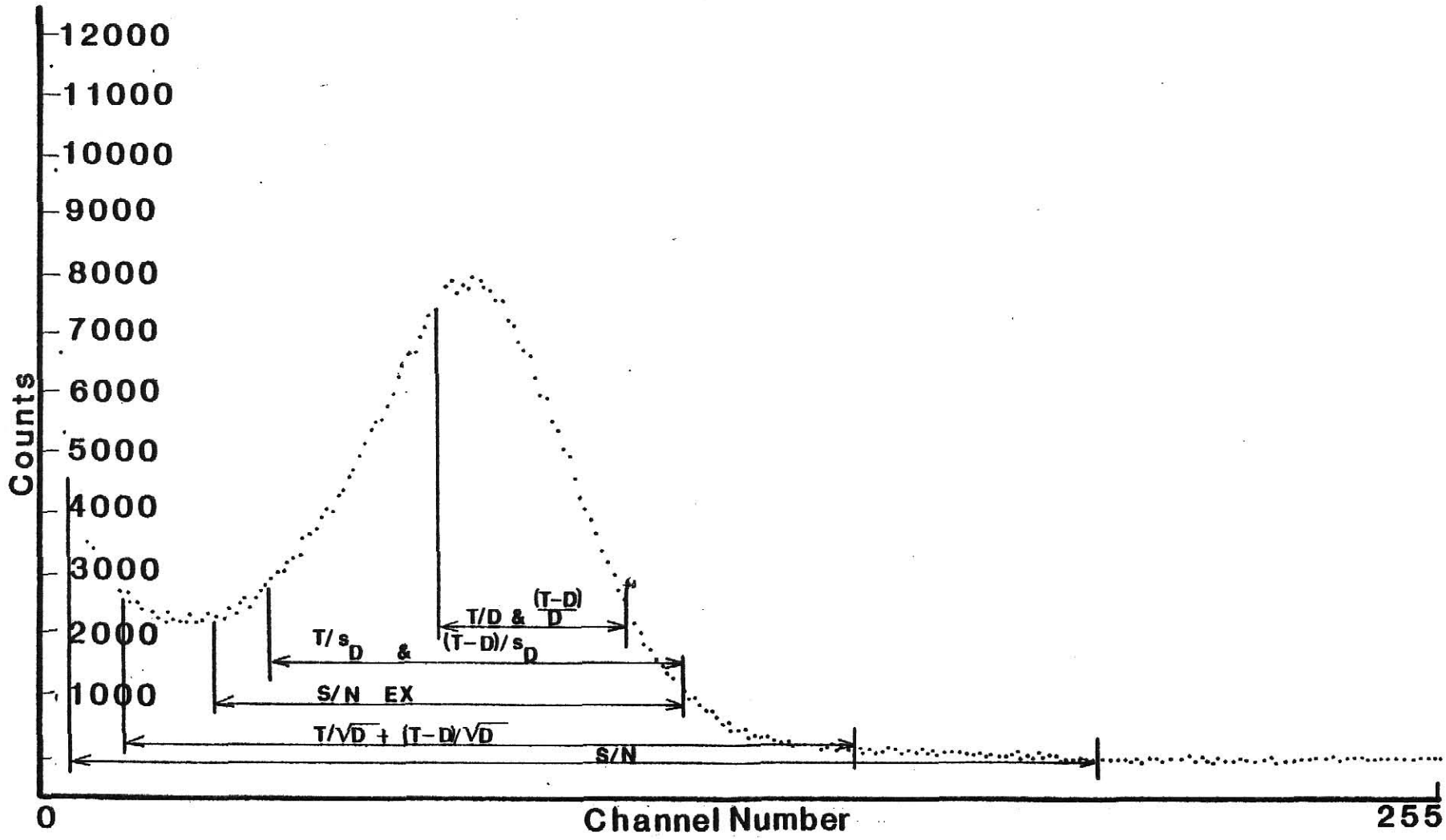

Fig. 5-4. A light differential pulse height distribution showing the optimum upper and lower discriminator levels for the performance ratios described in Section 5.2. (HV=2200 V, LED current=1.00 μA)

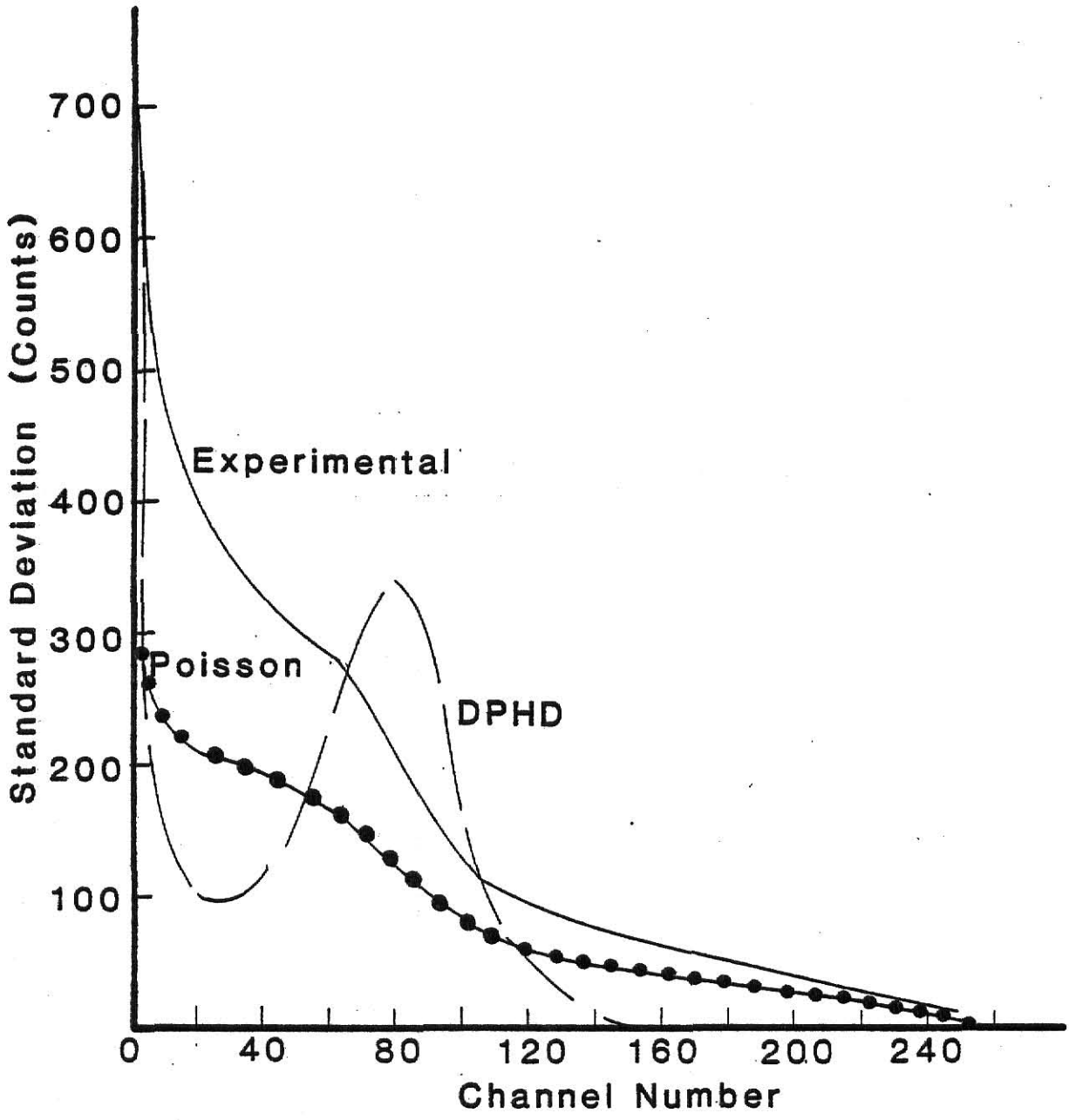

Fig. 5-5. Comparison of the Poisson and experimental standard deviations for a dark differential pulse height distribution as a function of LLD (channel number). (HV=2200 V, LED current=1.00 μA)

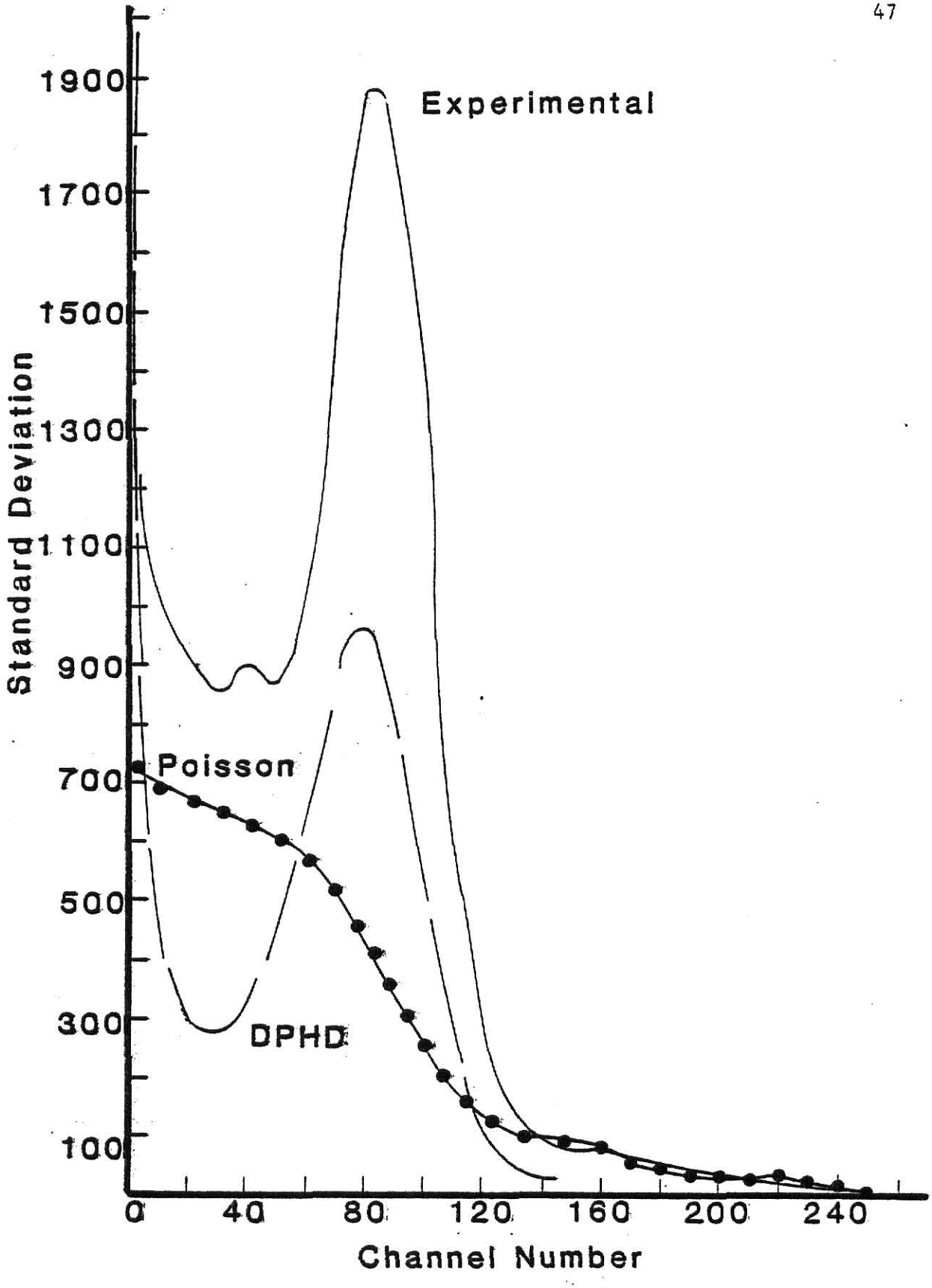

Fig. 5-6. Comparison of the Poisson and experimental standard deviations for a light differential pulse height distribution as a function of LLD (channel number). (HV=2200 V, LED current=1.00 μA)

As can be seen from Fig. 5-4, the peak of the DPHD is not a smooth curve but contains significant fluctuations. When more than one DPHD is used in order to calculate variance (s_T^2), these fluctuations will occur in different channels in the DPHDs causing a larger variance. This causes especially large variances in the peak area because here the counts in just one channel may be a significant portion of the entire integral PHD. In any respect, Poisson assumptions are obviously inaccurate.

As part of the work described above, an attempt was made to compare the maximum value of S/N EX for different values of HV in order to select an optimum value of this parameter. This, however, proved ineffective because a change in HV changed the pulse height gain, necessitating a compensatory gain change in the spectroscopy amplifier. In addition to the difficulty of compensating accurately, the spectroscopy amplifier added noise to the signal when operated at high gain. This noise was recorded as small pulses thus distorting the lower end of the DPHD. Due to these problems encountered when using the MCA to select the optimum HV, it was decided that the PAR units would be used instead. Because the PAR units were to be used more frequently than the MCA during ordinary TLD analysis, this was probably the more appropriate, if less elegant, method of selecting the optimum HV.

The design of the amplifier-discriminator unit was found to be the most influential factor in determining the optimum HV and discriminator levels. The amplifier preceeding the discriminator has five possible gain settings: 0.10, 0.33, 1.00, 3.33, and 10. The LLD ranges from 0-10 mV. The ULD is set by indicating the span (0-10 mV) desired

between the upper and lower level discriminators. The most desireable setting of the LLD, for any amplifier gain, was determined to be 2.75 mV because of the oscillation problems discussed in Section 4.6.2. The most desirable ULD setting was found to be 11.25 mV (an 8.5 mV span) because larger values were off-scale in the amplifier-discriminator's PHA mode. The optimum locations for the LLD and ULD were already known from the MCA tests to be in the DPHD valley and at the opposite base of the DPHD peak, respectively (See Fig. 5-4). Thus, the procedure for obtaining optimum operating conditions for a selected gain was as follows: 1) Set the LLD and ULD at 2.75 and 8.5 mV respectively. 2) Using the PHA mode, adjust the HV until the DPHD peak has been positioned between the discriminator levels so that the LLD is in the valley and the ULD is at the opposite base of the peak.

Using the above procedure there is one optimum value of HV for each choice of amplifier gain. Table 5-1 shows the five choices of amplifier gain, the corresponding value of HV, and the values of the performance ratios obtained under the specified conditions. All that remains in determining the optimum operating conditions for HV and discriminator levels is to select the amplifier gain and corresponding HV which give the highest value of S/N EX. From Table 5-1 or Fig. 5-7, which is a plot of S/N and S/N EX as a function of HV, the optimum amplifier gain is 1.00 with HV = 2120 V.

5.4 System Stability

When selecting optimal values of operating parameters another characteristic which should be considered in addition to SNR is system

Table 5-1. Optimization data for the amplifier-discriminator's gain and corresponding high voltage taken with an LED current of 1.00 μA and discriminator levels of 2.75 and 11.25 mV.

Parameter	Amplifier Gain				
	10.00	3.33	1.00	0.33	0.10
High Voltage	1710 V	1905 V	2120 V	2360 V	2595 V
S/N	194.86	194.46	191.56	187.87	154.15
S/N EX	85.04	152.74	187.83	93.99	101.66
T/D	13.08	11.73	9.84	7.83	3.75
(T-D)/D	12.08	10.73	8.84	6.83	2.75
$T/D^{\frac{1}{2}}$	791.76	758.55	702.03	640.06	458.12
T/s_D	305.52	318.44	423.77	422.29	175.89
$(T-D)/D^{\frac{1}{2}}$	731.23	693.89	630.68	558.33	335.93
$(T-D)/s_D$	282.17	291.29	380.71	368.37	128.98

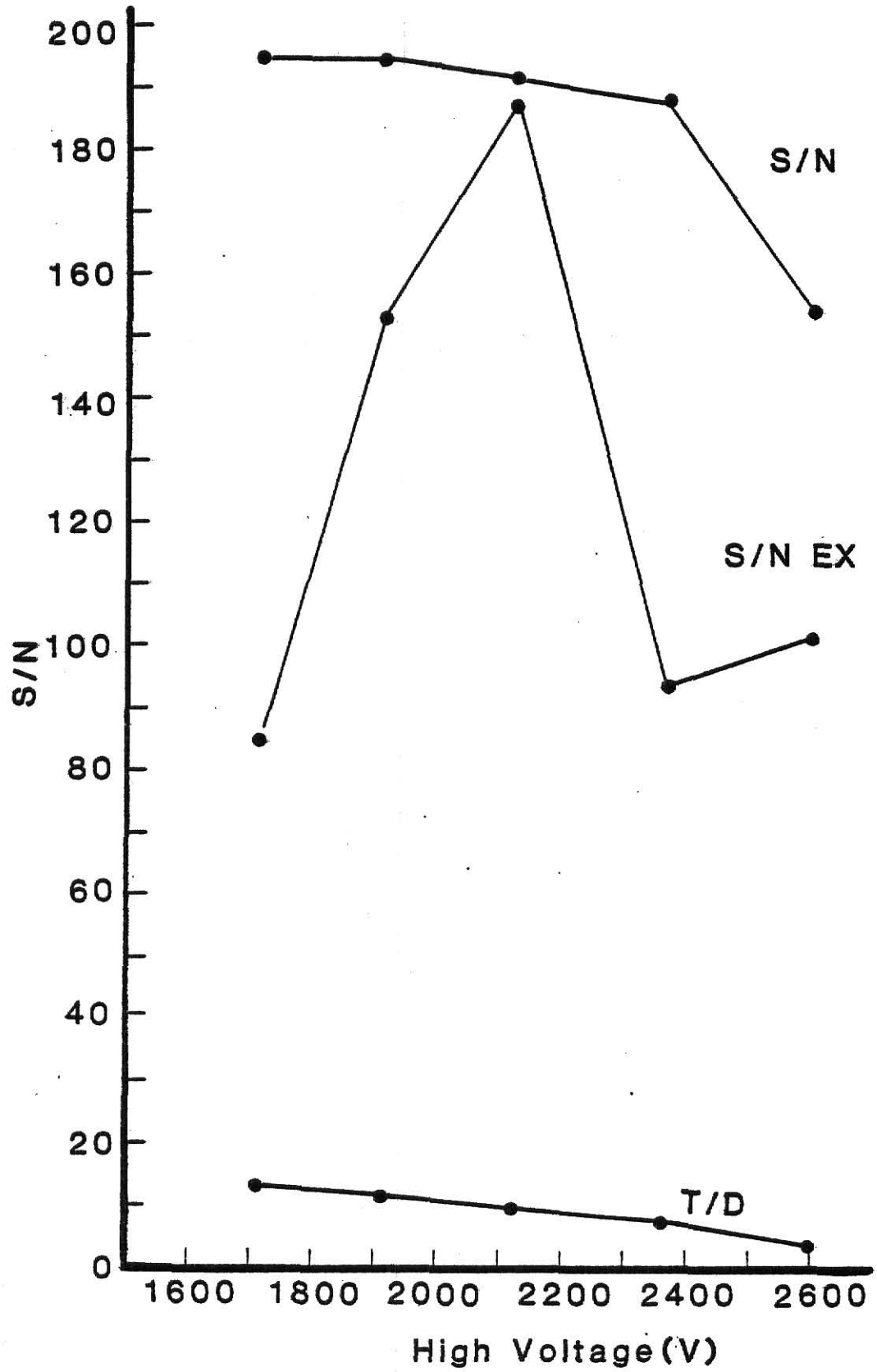

Fig. 5-7. Plot of S/N and S/N EX as a function of HV for the optimization of HV using the amplifier-discriminator.

stability. A system with good SNR but poor consistency on a day to day basis is of little practical use.

The optimum positions for the discriminator levels - with respect to stability - are the valley of the DPHD for the LLD and the base on the opposite side of the peak for the ULD. The reason for this is that if one of the discriminator levels or the gain drifts slightly, the number of counts within the discriminator window will not change significantly. However, if one of the discriminator levels is set high on the side of the peak, a shift in gain or discriminator level can make a noticeable change in the number of counts recorded within the discriminator window. This concept is illustrated for an exagerated case in Fig. 5-8. In Fig. 5-8a the discriminators are placed correctly so a shift in gain causes a relatively small change in the area under the curve between discriminator levels. Figure 5-8b shows the effect of the same gain change when the discriminator levels are improperly placed - the area under the curve changes significantly between the LLD and the ULD. From the above it is evident that the selected discriminator levels not only give the optimum value of S/N EX, but also provide optimum stability.

To test the system's stability under conditions of changing gain and discriminator level, the following tests were performed: With the LED light source being driven at 1.00 μA, ten 100 second counts were taken and averaged at the nominal settings of HV = 2120 V, LLD= 2.75 mV, and ULD = 11.25 mV. Then, while holding all other parameters constant, the LLD was increased to 3.0 mV and the test repeated. Next the LLD was decreased to 2.5 mV for another test. Likewise, tests were

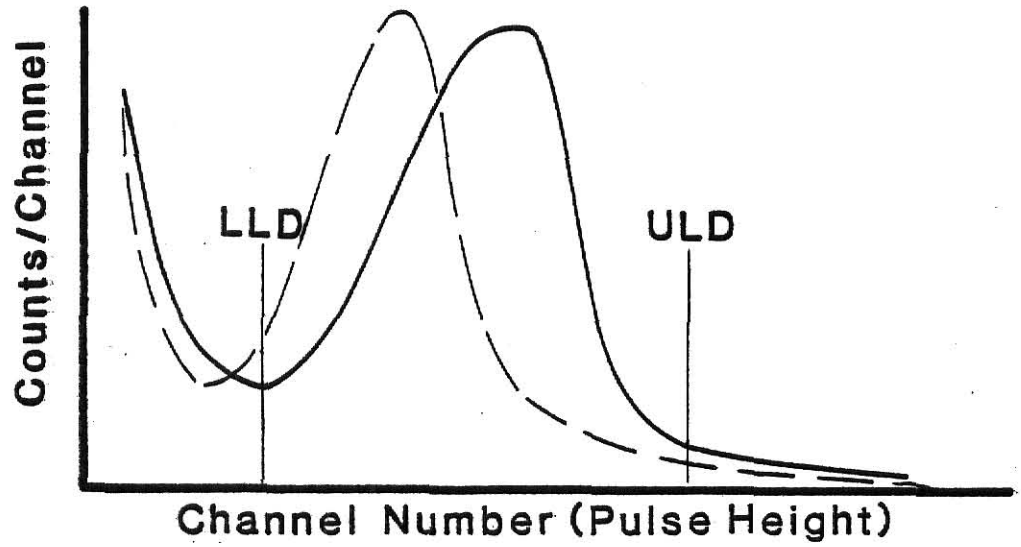

(a)

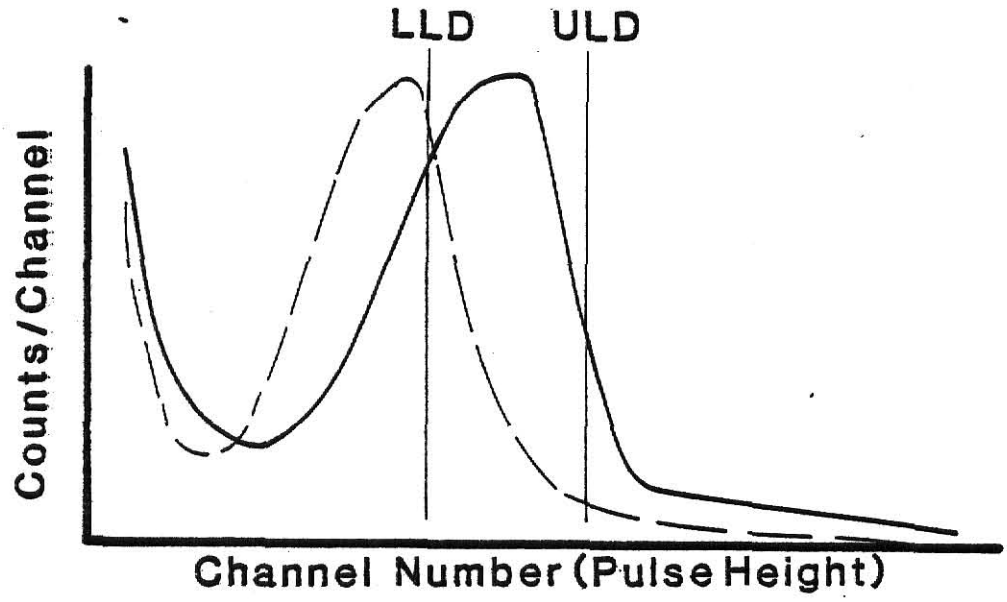

(b)

Fig. 5-8. The effect of a gain shift on the total number of counts recorded for: a) correctly placed discriminator levels, and b) incorrectly placed discriminator levels. Solid lines indicate the original DPHD, dashed lines represent the shifted version.

performed with the ULD at 10.75 mV and 11.75 mV, and with HV at 2115 V and 2125 V. Table 5-2 shows the changes in HV and discriminator level and the resulting percent change in the average number of counts collected. The data indicate that stability is most dependent on the LLD, where a change of 0.25 mV (9% from nominal) results in the average number of counts changing by approximately 1.4%. This is still very good - a given percent change in discriminator level causes a change less than one sixth as large in the average number of counts collected.

The first experiment performed to monitor the system's long term stability utilized the LED light source. With the LED on, the count rate was recorded by directing the pulses from the PMT to the multiscaling MCA input. In the multiscaling mode the analyzer counts the number of pulses arriving within a given dwell time, records them in the current channel, and then advances one channel to repeat the procedure. Using this arrangement, data were collected for approximately 60 continuous hours in 4096 analyzer channels. The resulting data showed only the expected statistical fluctuation about the mean. There was no detectable trend of either an increase or decrease in the number of counts per channel.

The system's stability was also checked under normal operating conditions by reading out sets of TLDs daily for five days. All TLDs used in this experiment received the same dose, approximately 100 mrad. A linear least squares fit was performed on the resulting data plotted as the average number of counts recorded as a function of the day of readout. The slope of the line fit to the data was -20.4 counts/day or, dividing by the mean number of counts per readout, a -0.07% change in

Table 5-2 Data for determining the photon counting system's sensitivity to small changes in high voltage and discriminator levels.

High Voltage (V)	Lower level Discriminator (mV)	Upper level Discriminator (mV)	Percent change in number of counts collected
2120	2.75	11.25	———
2120	2.50	11.25	+1.07
2120	3.00	11.25	-1.37
2120	2.75	10.75	-0.45
2120	2.75	11.75	+0.46
2115	2.75	11.25	-0.03
2125	2.75	11.25	+0.49

the average number of counts recorded per readout per day. All five points were also within four percent of the mean value - a typical spread for a set of TLDs all analyzed on the same day. The conclusion drawn from these two experiments was that the system is stable enough to be useful and accurate on a long term basis.

5.5 Optimization of the Temperature Window

The sensitivity of a TLD analysis system may also be improved by collecting data only during a specified temperature interval of the heating cycle. The desired portion of the output (as a function of temperature) occurs as a thermoluminescence peak, as described in Chapter 2. The objective in selecting a temperature window is to determine an optimum upper and lower temperature (T_2 and T_1) which describe the window giving the best system sensitivity.

This idea is similar to that of using pulse height discrimination to optimize the SNR. In fact, if a TLD is read out two times consecutively, the first result can be considered the light or total distribution while the second is the dark or noise component. By operating the MCA in the multiscaling mode with the PMT output connected to the multiscaling input on the MCA, the glow-curve shown in Fig. 5-9 was obtained. With this data recorded on magnetic tape, the program OPTPC was used to find the values of T_1 and T_2 which gave the optimum SNR. These values occured where expected and are indicated on Fig. 5-9 for the specific case of a ^{7}LiF TLD which absorbed approximately 25 mrad and was heated at a rate of 5°C/sec. Unfortunately, the peak width (and

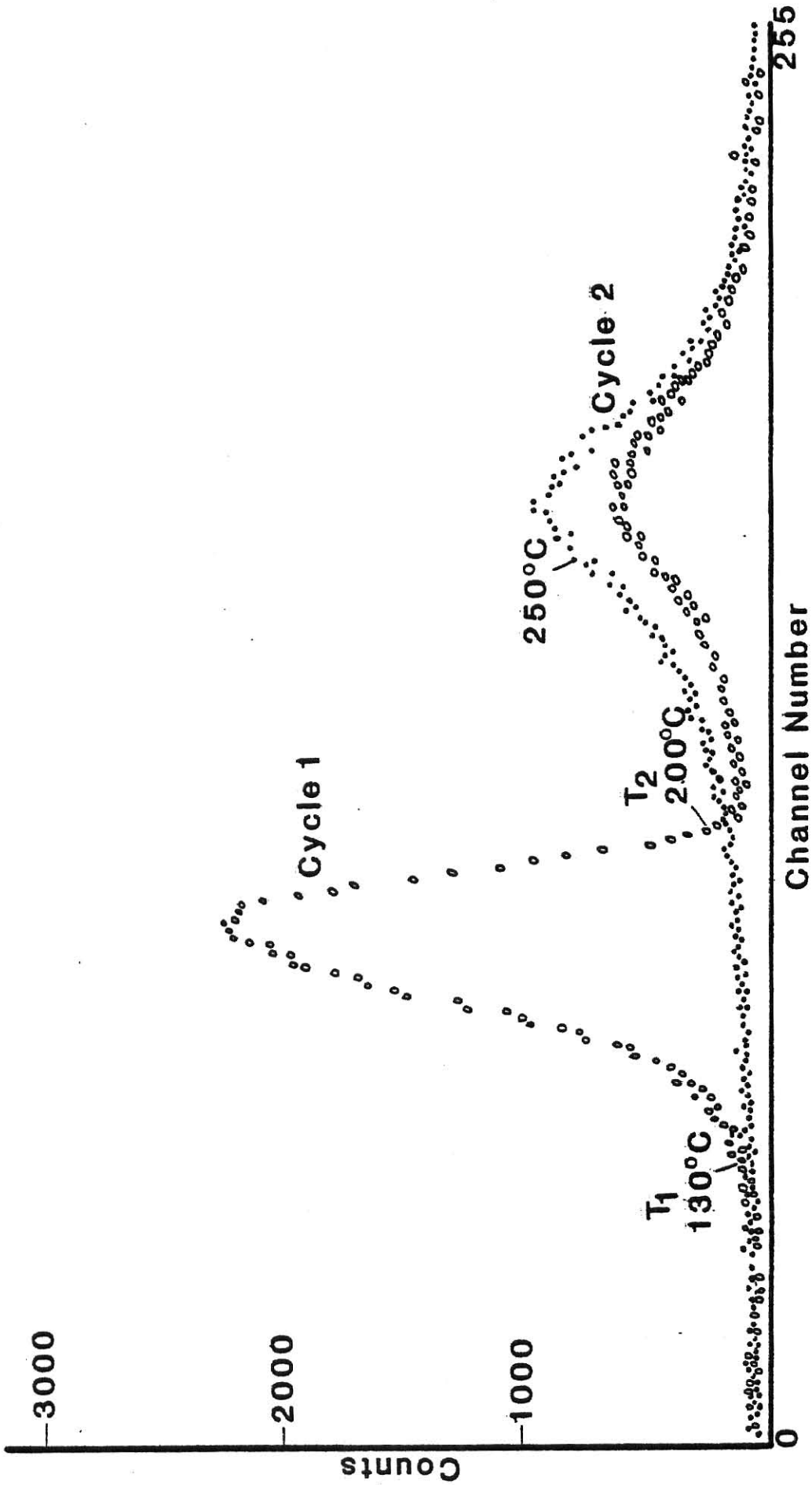

Fig. 5-9. The glow curve for a LiF TLD heated at $5^{o}C$/sec showing the optimum values of T_1 and T_2.

thus the optimum window width) increased with increasing dose. Therefore, a window corresponding to relatively large doses was used for all TLD analysis. The values of T_1 and T_2 for ^7LiF were 130°C and 200°C respectively, while those for CaF_2:Mn were 150°C and 250°C.

After determining the optimum values for the temperature window it was also necessary to select a TLD heating rate. Hanna (9) reported that a slower rate (12.5°C/sec as opposed to 24.7°C/sec) gave better reproducibility and extended the system's linear dose range from 40 rads (rate = 24.7°C/sec) to 100 rads (rate = 12.5°C/sec). The disadvantage of making the heating rate slower is that the readout process becomes longer. As a compromise between the convenience of a short readout cycle and the improved performance of a slow heating rate, 5°C/sec was chosen as the TLD heating rate.

6.0 Experimental Procedures

When using TLDs for absorbed dose analysis, the procedures used in every step of the annealing, irradiation, and readout processes can have an impact on the final result and therefore should be specified. This chapter describes the experimental procedures used in this work.

6.1 TLD Selection

Both the set of Harshaw ^{7}LiF (TLD-700) and Harshaw CaF_2:Mn (TLD-400) 1x1x6 mm TLD rods had been previously selected for a low dose experiment by a simple presort procedure (43). Two hundred new TLDs were first sorted by physical appearance, with any which appeared broken or chipped being discarded. Next, the remaining TLDs were irradiated so that each received the same gamma dose. These TLDs were then read out on a commercial TLD reader. The mean of all the readouts was calculated and then every TLD which fell outside of the range of ± 5% from the mean was discarded.

6.2 Irradiations

Three different sources were used for irradiating the TLDs. A 5 mCi Co-60 source, traceable to the National Bureau of Standards, was used for low dose experiments. The second source was a 5 Ci Co-60 pumped source. This source, intercalibrated with the 5 mCi source, was used to obtain data in the intermediate dose range. Finally, the KSU gammacell, capable of dose rates of approximately 470 rad/min., was chosen for high dose studies.

Before the gammacell could be used accurately it was necessary to calculate the dose received while the TLDs were being cycled in and out of the irradiation cell. This was done using the TLDs and the calibration obtained with the 5 mCi source. The transit dose was calculated to be approximately 22.5 rad.

Irradiations with the 5 mCi and 5 Ci sources were performed on sheets of styrofoam to reduce backscatter. The sheets were normally suspended during irradiation to reduce backscatter from floors and table tops. Slight indentations in the form of concentric circles, with radii from 10 to 40 cm from the source, were used to keep the TLDs in place during irradiation.

Prior to irradiation, all TLDs were placed in cylindrical stainless steel sleeves with inner and outer diameters of 0.142 cm and 0.318 cm respectively. Assuming that electronic equilibrium was established between the TLD and the stainless steel, the light emission from the TLD could be correlated to the absorbed dose in stainless steel.

6.3 TLD Handling

The following set of TLD handling procedures were developed to retain the identity of each individual TLD and to minimize errors introduced by inconsistent handling.

When not in stainless steel sleeves or glassware for annealing, each TLD was kept in an individual coin envelope for identification. All transferring and handling of TLDs was performed with tweezers tipped with shrink-fit tubing. This was to prevent scratching the dosimeter surfaces which reduces the thermoluminescence (TL) output. Cox et al

(44) reported that TLDs handled with metal tweezers became slightly more opaque with use. Microscopic observation showed the opacity was attributable to numerous tiny scratches on the dosimeter's surface.

The washing procedure mentioned in Chapter 2 was used during some of the low dose measurements prior to readout. The wash, developed by Spanne (45) and tested by Driscoll and McKinlay (11), consists of immersing the TLDs for several seconds in a solution of HCl: methanol in the proportion 1:83. For this work the wash was followed by a rinse in pure methanol.

6.4 Annealing

The annealing procedure which was used is that described in Chapter 2. Prior to irradiation the TLDs were annealed in a 400°C oven for one hour, followed immediately by a two hour anneal at 100°C. A post-irradiation anneal of 10 min. at 100°C was also used. All TLD annealing procedures were performed in Pyrex glassware.

6.5 Exposure to Background Radiation

Attempting to record very low doses with TLDs exposed to the 5 mCi source proved to be impractical. Even at 40 cm, the most remote distance from the source on the irradiation device, only 13 seconds were required to accumulate a dose greater than 100 μrads. With such short irradiation times the uncertainty introduced during the placement and removal of the source was unacceptably large. It was decided that the best way to test TLD response to small doses was by exposure to background radiation for varying lengths of time. To this end, as soon as

the TLDs were removed from the 100°C oven they were placed in their stainless steel sleeves and left on a table in a darkened room. Every two hours a set of five TLDs were washed and read out. Care was taken to minimize the effects of room lighting on TLD response by using only one incandescent light. The background exposure rate was monitored with a Reuter Stokes RSS-111 Environmental Radiation Monitor. This device did not have an integration mode so a record of total dose was not available. However, the background rate was monitored continuously and was approximately 9.5± 0.5 μR/h for the duration of the tests.

6.6 Optimization of the Commercial Unit

A comparison of the photon counting system and a standard Harshaw system consisting of the 2000A TL Detector and the 2000B Integrating Picoammeter was performed. It is important to note that this was <u>not</u> a direct comparison of photon counting to DC techniques which would require using the same system in both modes. It was merely a test to see how the photon counter compared to a typical commercial system presently in use.

Before running the comparison it was necessary to optimize the commercial system. This was done by collecting S/N EX data similar to that for the photon counter (see Chapter 5), with two main exceptions: 1) Instead of counting pulses, an amount of charge was measured which should be directly proportional to the number of pulses coming from the PMT. 2) In the DC mode it was not possible to employ discriminators so data were taken only as a function of HV. The optimum value of HV resulting from this test was 725 V.

6.7 Noise Subtraction Using the Second Read

Based on the results of previous experiments (9,46), the photon counting system was originally designed to readout each TLD twice to allow the second reading (background) to be subtracted from the first. It was hoped that all chemiluminescence, planchet emissions, and PMT dark noise would be the same for both cycles, allowing one to subtract the output caused by these effects from the desired signal. However, when this technique was applied to TLDs with background level exposures the second read was consistently higher than the first.

Figure 6-1 shows the glow peak portion of a typical glow curve for both cycles. From this figure it appeared that part of the problem may have been that the second read began with the TLD (not the planchet which was monitored by the thermocouple) at a higher temperature than in the first cycle. To investigate this possibility, each TLD was read out once, allowed to cool at room temperature for approximately 20 minutes, and then readout again. This time the difference in the two glow curves was not as apparent but the mean number of counts for each set of TLDs was still consistently higher on the second cycle. For this reason the second cycle was eliminated. If an estimation of the zero dose reading is required, the most accurate estimate can be made by extrapolation from the low dose data.

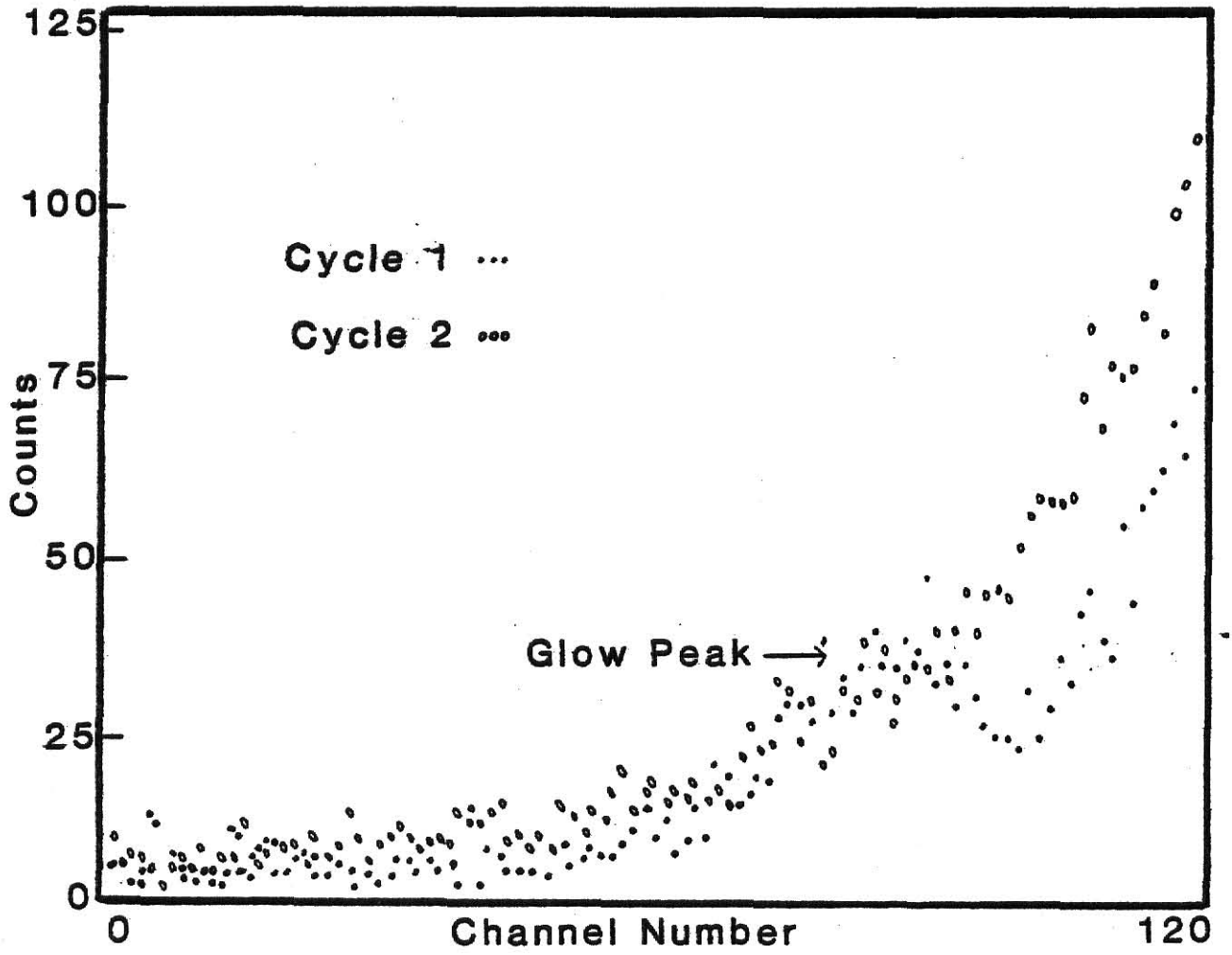

Fig. 6-1. Comparison of the glow curves obtained for the first and second read of a LiF TLD which absorbed approximately 150 μrads.

7.0 Results

Data presented in this chapter are representative of the results obtained from a series of experiments designed to test the photon counting system's range and accuracy. All experiments were performed using the optimal parameters found in Chapter 5 and the procedures described in Chapter 6.

7.1 Initial Range Test

A range test was first performed to find the approximate upper and lower dose limits of the system, and its linearity in between, using ^{7}LiF (TLD-700) dosimeters. Later sections in this chapter will describe tests used to determine the upper and lower limits more precisly and how they might be improved.

The results of the range test are presented in Table 7-1 and Fig. 7-1. Looking at Fig. 7-1 it appears that the system has good linearity between approximately 2×10^{-3} to 50 rads. At doses above 50 rads the curve becomes nonlinear due to pulse pileup caused by extremely high counting rates. The apparent nonlinearity at the lower end is somewhat deceiving in that it is the result of plotting a function with a nonzero intercept on a log-log scale and does not necessarily indicate data nonlinearity.

7.2 Dead Time Determination

Dead time losses occur when two or more pulses are too close together to be recorded as separate pulses. This minimum time separation, necessary for distinguishing the two pulses, is known as dead

Table 7-1. Dose and corresponding average readout obtained in the initial range test.

Dose (rads)	Average Readout (counts)	Standard Deviation (percent)
455	323,724,982	1.2
377	318,129,508	0.9
298	308,633,796	2.0
219	264,583,152	0.7
145	219,647,828	2.9
69.8	134,594,070	2.5
57.9	122,699,858	3.5
46.1	104,957,972	2.8
37.1	91,164,124	1.8
30.4	79,732,682	0.8
22.6	57,514,758	3.8
17.2	44,038,994	1.5
9.37	24,157,905	0.6
1.04	2,741,944	4.6
85.8 (10^{-3})	234,194	3.5
16.5 (10^{-3})	48,316	1.3
5.04 (10^{-3})	13,211	2.0
1.38 (10^{-3})	4,557	2.6
894 (10^{-6})	3,705	7.4
624 (10^{-6})	2,980	5.3
354 (10^{-6})	2,663	11.4

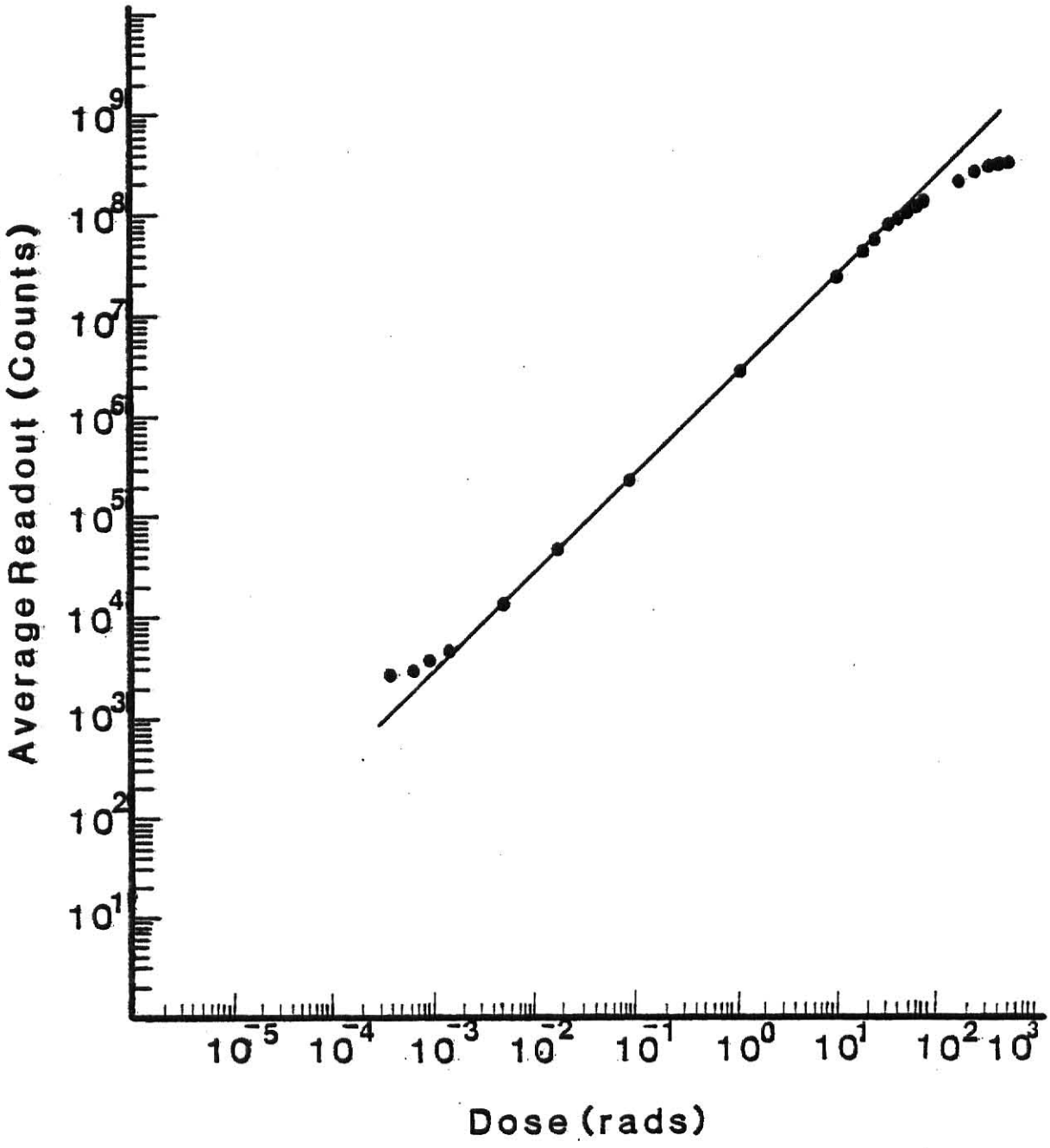

Fig. 7-1. Log-log plot of the dose vs. readout data obtained in the initial range test.

time. The effect which dead time will have on the output of a pulse counting system depends upon which dead time model the system most closely resembles - paralyzable or nonparalyzable.

The paralyzable model assumes that after each pulse there is a fixed dead time (τ) during which no additional pulses may be recorded and that any additional pulses in this period extend the total dead time by an amount τ from the time when the additional event occurred. The nonparalyzable model assumes that any pulses occurring while the system is dead are ignored. This means the total dead time cannot be extended as is the case with a paralyzable system.

According to the PAR manual(34), the amplifier-discriminator unit is nonparalyzable while PMTs are paralyzable. The manual also lists the dead time of the amplifier-discriminator as 5 ns while reporting that most PMTs have dead times greater than 10 ns. Therefore this system was assumed to be paralyzable.

Once the dead time and the appropriate model have been determined a correction may be applied for dead time losses according to the formulas(47):

$$\text{Paralyzable} \qquad m = ne^{-n\tau} \tag{7-1}$$

$$\text{Nonparalyzable} \qquad n = \frac{m}{1-m\tau} \tag{7-2}$$

where

n = true interaction rate

m = recorded count rate

τ = system dead time.

The method used to measure the dead time, known as the two source method, is generally used to measure dead time in radiation detectors. But this is a light detection system, so a light source taken from a commercial TLD reader was used instead. The source was split into two pieces. Then the count rate was determined for each piece separately under the PMT and then for both together under the PMT. Because the counting losses are nonlinear, the observed rate due to the combined sources was less than the sum of the rates due to the two sources counted individually. This discrepancy was used to determine the dead time from the following equation (47):

$$n_{12}-n_b = (n_1-n_b) + (n_2-n_b) \ . \qquad (7\text{-}3)$$

n_1, n_2 ,n_{12}, and n_b represent the time interaction rates due to source 1, source 2, the combined sources, and background respectively. These may be found from either Eq. (7-1) or (7-2) by using the measured values m_1, m_2, m_{12}, and m_b.

Using the paralyzable model in Eq. (7-3) required an iterative technique due to the transcendental nature of Eq. (7-1). This was done using the data in Table 7-2 with the result being τ = 13.0 ns.

Unfortunately, the glow curve in Fig. 5-9 indicates that the count rate during readout will change quite drastically in the area of interest because of the glow peak. This means Eq. (7-1) would have to be

Table 7-2. The measured counting rates - for source 1, source 2, the combined sources, and background - used in determining system dead time.

Trial	Count rate for Source 1: m_1 (counts/second)	Count rate for Source 2: m_2 (counts/second)	Combined Source Count rate: m_{12} (counts/second)	Background Count rate: m_b (counts/second).
2	8,692,353	9,907,405	16,187,780	127
3	8,680,837	9,901,028	16,179,752	124
4	8,680,768	9,893,660	16,182,453	118
5	8,680,416	9,885,322	16,171,727	134
Average	8,686,753	9,906,496	16,183,835	136
Standard Deviation	0.1%	0.2%	0.06%	18%

applied to each point on the glow curve individually before summing the results in order to obtain a valid correction. This was not feasable but it was relatively simple to calculate a bench mark value to indicate the system's limitations. For example, the instantaneous count rate which would cause a 5% dead time loss in the readout was calculated to be approximately 388×10^6 counts/sec.

7.3 Extension of Upper Dose Limit Using Optical Filters

One objective of this research was to experiment with the use of neutral density optical filters to extend the photon counting system's useful range. By placing a neutral density filter next to the infrared filter in the holder shown in Fig. 4-7 the intensity of the light reaching the PMT may be reduced. This would not be desirable when working with small or unknown doses but could be helpful when doses are known to exceed a specified value. Table 7-3 and Fig. 7-2 present a comparison of the upper limit of the system with and without a 2.0 optical-density neutral-density filter. (More precisely, at a wavelength of 400 nm this filter transmitts 1.26% of the light incident on its surface.) The figure shows that the output becomes nonlinear at approximately the same count rate (10^8-2×10^8 counts/readout) whether or not the filter is present. But by attenuating the light signal incident on the PMT the corresponding dose limit has been increased from approximately 50 rad to 3000 rad.

Note that without the filter, nonlinearity of the system occurs before the TLD response becomes supralinear. With the neutral density

Table 7-3. Data used in the comparison of the system;'s upper dose limit with and without the neutral density filter (1.26% transmission at 400nm).

Dose	NO FILTER		FILTER	
	Average Readout	Standard Deviation	Average Readout	Standard Deviation.
(rads)	(counts)	(percent)	(counts)	(percent)
17.2	44,038,994	1.5		
22.6	57,514,758	3.8	1,052,638	2.6
37.1	91,164,124	1.8	1,751,492	3.1
69.8	134,594,070	2.5	2,945,914	1.6
148.5	219,647,828	2.9	5,815,600	2.7
219.3	264,583,152	0.7	8,746,074	3.6
297.9	308,633,796	2.0	12,316,988	5.6
376.6	318,129,508	0.9	15,445,106	4.7
400.0	---	---	16,761,500	5.2
455.3	323,724,982	1.2	19,090,375	2.5
800.0	---	---	36,013,548	2.5
1300	---	---	59,465,218	2.1
2000	---	---	93,534,896	4.3
4000	---	---	175,477,478	2.3
6000	---	---	248,739,604	1.1
8000	---	---	294,090,664	1.3
10,000	---	---	312,623,218	1.5

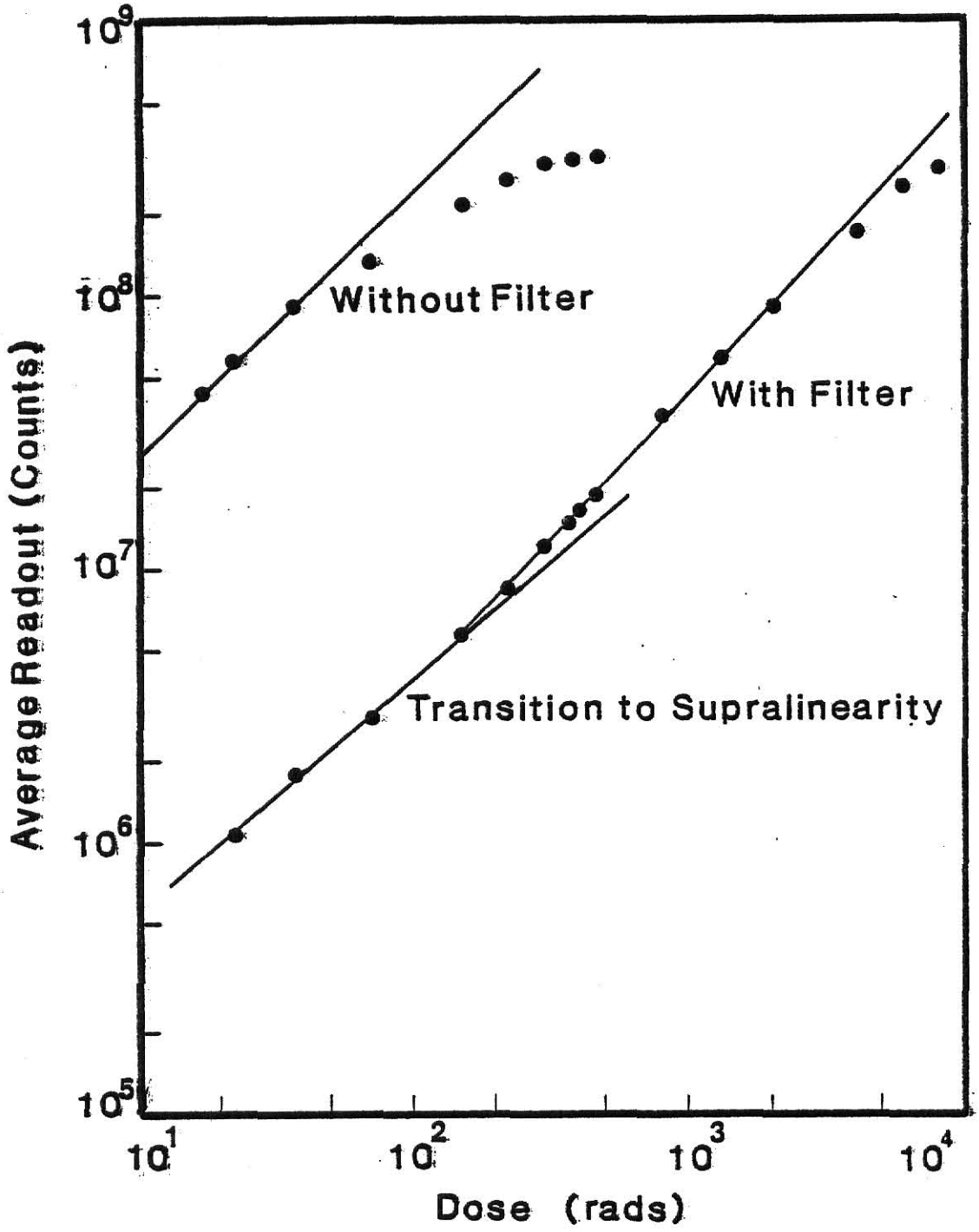

Fig. 7-2. Graphical comparison of the system's upper dose limit with and without the neutral density filter (1.26% transmission at 400 nm).

filter in position, however, the increase in slope - which indicates supralinearity - occurs before the system reaches its upper limit of linearity.

Based on these results, if the operator knows in advance that the absorbed dose was greater than, for example, one rad, the neutral density filter may be used to extend the systems useful range from 50 rad to 3000 rad. In addition, filters with higher optical densities could be used to extend the upper limit further - to the point where TLD response becomes saturated.

7.4 The Effects of TLD Washing on Low Dose Measurements

Two sets of data were taken with the LiF dosimeters to determine the effect of washing the TLDs. The first set of TLDs were processed in the usual way. The same procedure was followed for the second set, with the exception of washing the TLDs as described in Section 6.3 prior to readout. A comparison of the results obtained with both sets is shown in Table 7-4 and Fig. 7-3. From these results it is apparent that washing the TLDs greatly improves linearity at low doses. It should also be noted that although no quantitative measurements were made, it appears as if washing may cause a slight decrease in TLD sensitivity with repeated use.

7.5 Comparison of the Photon Counter to a Commercial DC System

Data measured with the commercial DC system, described in Section 6.6, were compared to results obtained with the photon counting system. This study was performed using washed LiF TLDs which had absorbed small doses and the readout process described previously.

Table 7-4. Comparison of the average readout obtained with unwashed TLDs and TLDs washed in acidic methanol.

Dose (mrads)	WASHED TLDs Average Readout (counts)	WASHED TLDs Standard Deviation (percent)	UNWASHED TLDs Average Readout (counts)	UNWASHED TLDs Standard Deviation (percent)
0.94	2627	5.9	3702	20
0.55	1947	4.0	2654	8.5
0.35	1490	3.6	2247	6.3
0.25	1273	9.1	2304	9.0
0.18	1154	16	1804	7.3
0.14	1082	15	2127	12
Linear Least Squares fit:	Readout = 806 + 1965(Dose)		Readout = 1622 + 2120(Dose)	
Correlation Coefficient:	0.9972		0.9336	

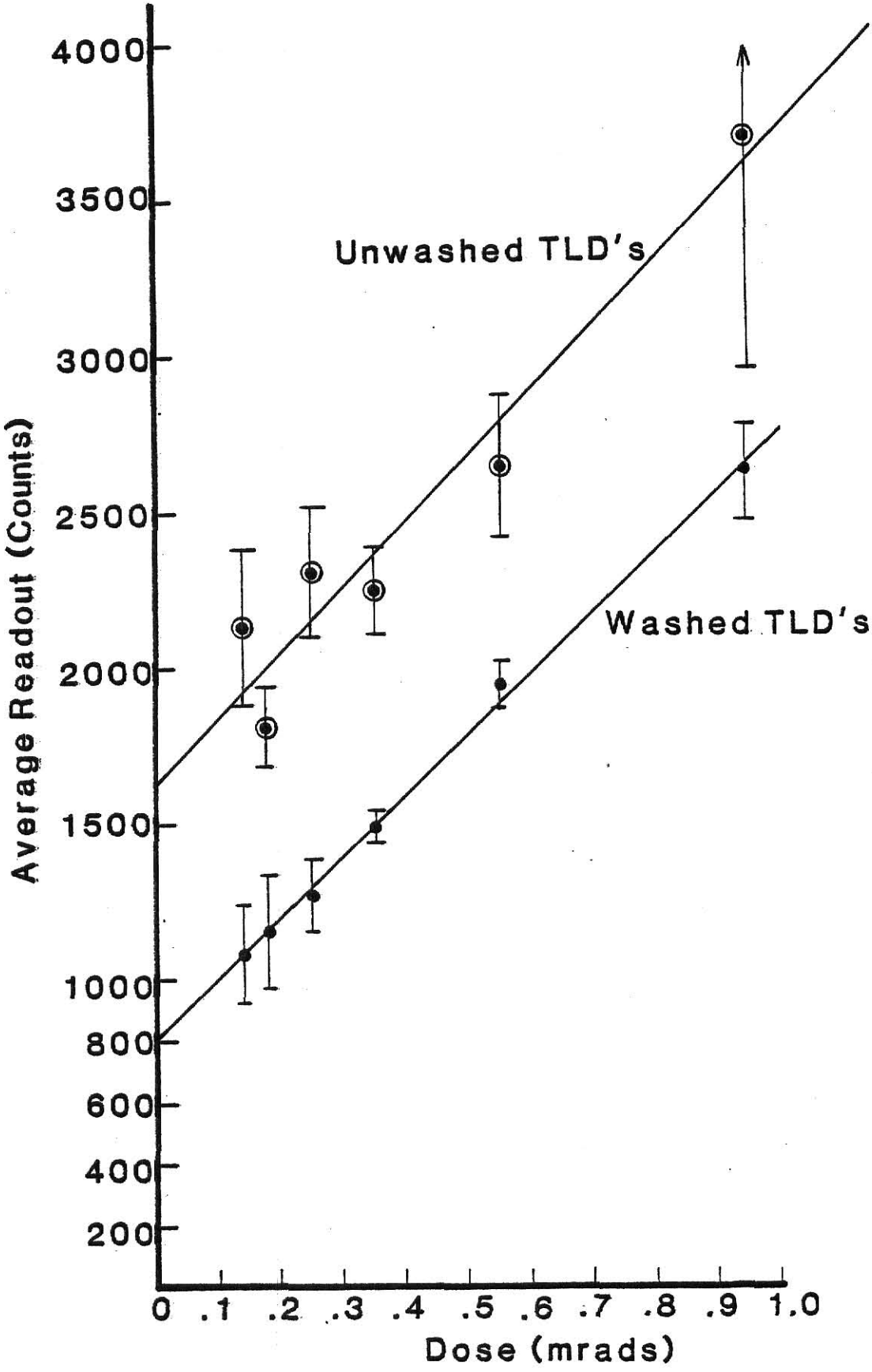

Fig. 7-3. Graphical comparison of dose vs. average readout data for unwashed TLDs and TLDs washed in acidic methanol.

The results, shown in Table 7-5 and Fig 7-4, indicate that the commercial unit's biggest shortcoming was its lack of precision. Only two digits are useful for low dose readouts and these varied by only 0.004 nC from 0.017 to 0.023 nC as the dose varied from 0.14 to 0.94 mrad. This problem is similar to quantization error in analog-to-digital converters when there are insufficient bits available to adequately represent the data. This problem also makes this particular commercial system virtually useless for doses below approximately 0.5 mrad.

7.6 Measurement of Background Exposure

The reasons and procedures for measuring background exposure with TLDs were given in Section 6.5. In addition to the ^{7}LiF (TLD-700) dosimeters used previously, a set of CaF_2:Mn (TLD-400) rods were exposed and analyzed. The results are given in Tables 7-6 and 7-7 and Figs. 7-5 and 7-6. The abscissas in these graphs are given as exposure time rather than absorbed dose. Time zero on the abscissas was defined as the moment when all the TLDs in the set had been removed from the 100°C oven, encased in their stainless steel sleeves, and placed on a table near the area radiation monitor. Assuming that the dominant source of background radiation was ^{40}K, the exposure time may be used to calculate the approximate absorbed dose using the expression:

$$\text{Dose}_{BG}(\text{in stainless steel}) = (7.8\ \mu\text{rad/h})(\text{time(h)}). \quad (7\text{-}4)$$

The results for both sets of TLDs (LiF and CaF_2:Mn) definitely show the linear increase of readout as a function of time which indicates the accumulation of a small background dose. Equation (7-4) implies that

Table 7-5. Data used to compare the photon counting system to a commercial DC TLD analyzer for low dose measurements.

	PHOTON COUNTER		COMMERCIAL DC	
Dose	Average Readout	Standard Deviation	Average Readout	Standard Deviation
(mrads)	(counts)	(percent)	(nC)	(percent)
0.94	2627	5.9	0.023	9.8
0.55	1947	4.0	0.020	3.5
0.35	1490	3.6	0.018	8.8
0.25	1273	9.0	0.018	12
0.18	1154	16	0.017	9.8
0.14	1082	15	0.018	8.8
Linear least Squares fit:	Readout = 806 + 1965(Dose)		Readout = 0.016 + 0.00705(Dose)	
Correlation Coefficient:	0.9972		0.9434	

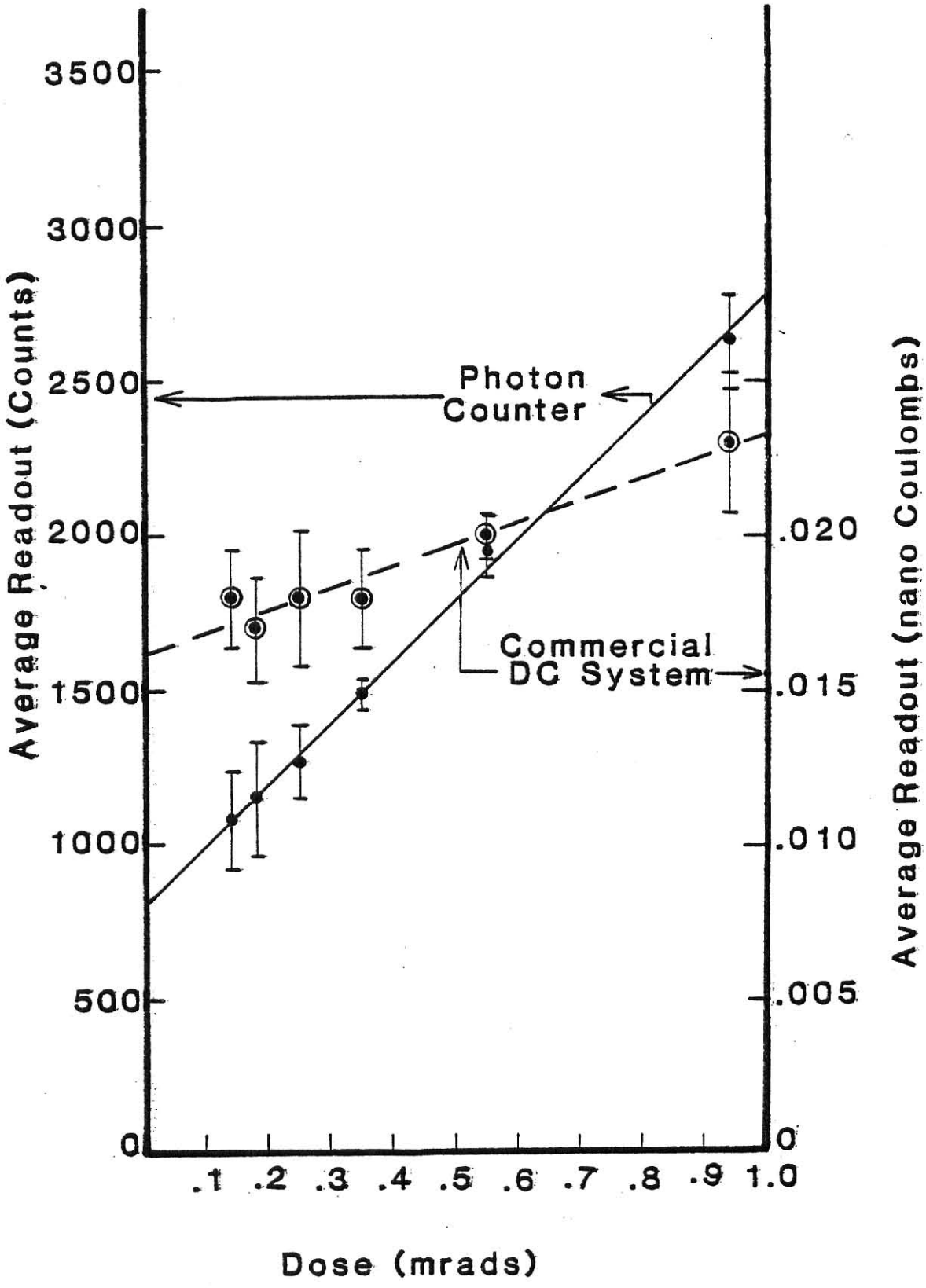

Fig. 7-4. Graphical comparison of the low level dose measurements made with the photon counting system and the commercial DC system.

Table 7-6. Average readout as a function of time for ^{7}LiF TLDs exposed to background radiation.

Time (minutes)	Average Readout (counts)	Standard Deviation (percent)
130	622	7.8
240	664	7.3
360	695	10.2
475	724	9.4
600	699	10.5
715	777	9.1

Linear least squares fit: Readout = 605 + 0.220(Time)

Correlation Coefficient: 0.8442

Table 7-7. Average readout as a function of time for CaF_2:Mn TLDs exposed to background radiation.

Time (minutes)	Average Readout (counts)	Standard Deviation (percent)
120	22911	2.04
242	23486	1.58
361	24010	1.79
491	24615	1.71
594	24924	2.01
718	24841	1.27

Linear least squares fit: Readout = 22659 + 3.498(Time)

Correlation coefficient: 0.9279

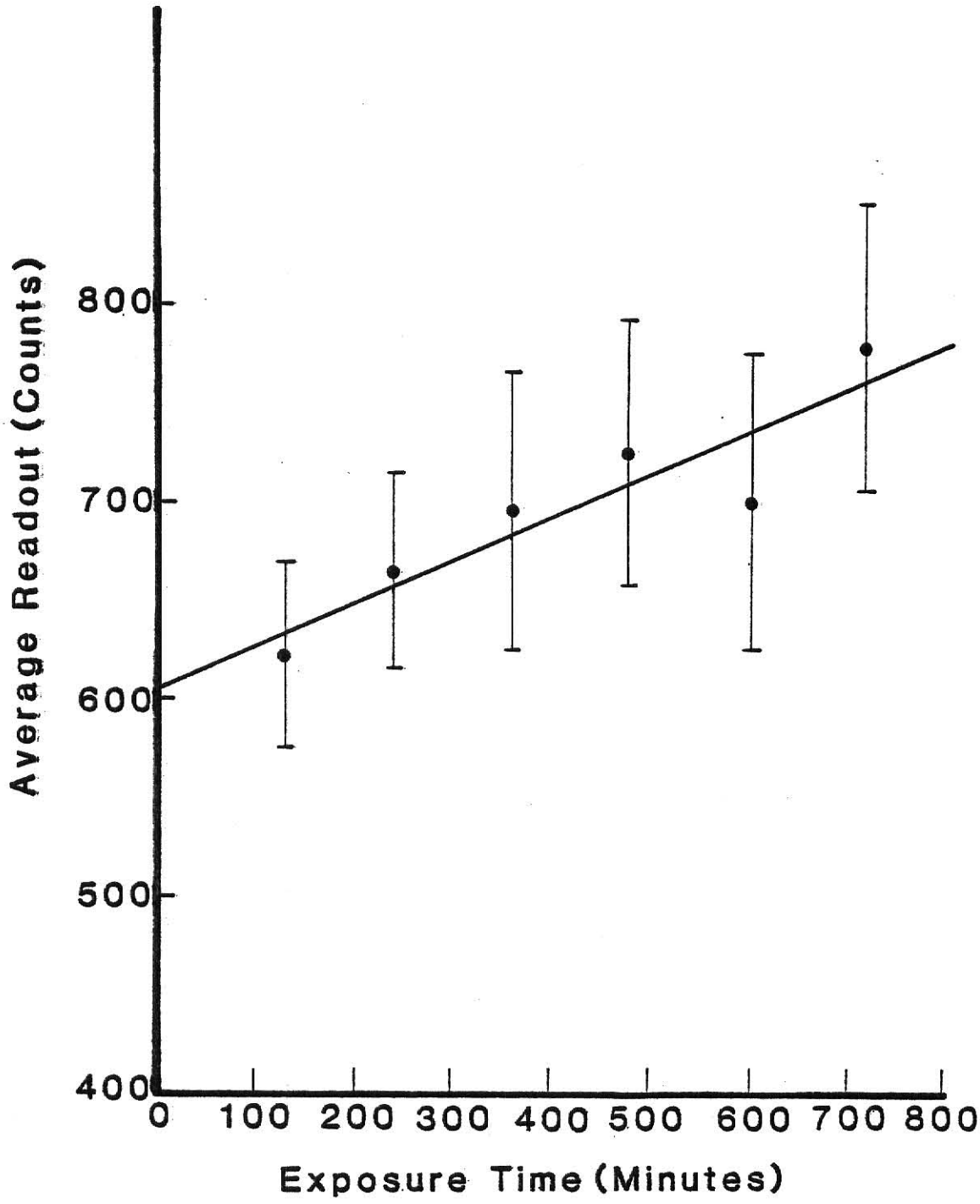

Fig. 7-5. Linear least squares fit to the readout vs. time data obtained by exposing ^{7}LiF TLDs to background radiation.

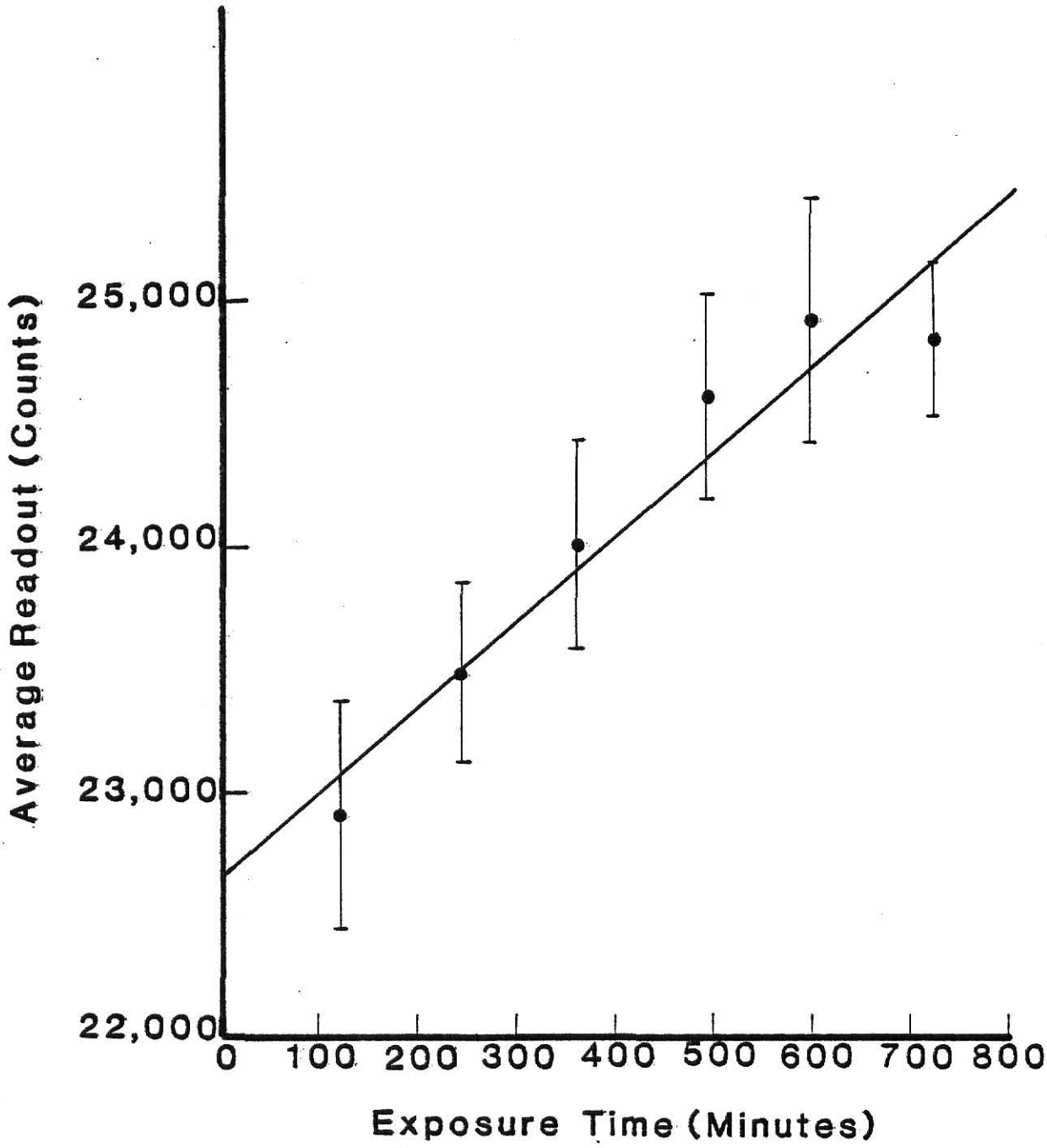

Fig. 7-6. Linear least squares fit to the readout vs. time data obtained by exposing CaF_2:Mn TLDs to background radiation.

the incremental dose being measured, corresponding to the approximate time interval of two hours, was 15.6 μrad. From the figures it appears that this dose increment was detected with acceptable accuracy for five of the six data points for both the LiF and CaF_2:Mn TLDs.

Comparing the linear least squares fits for LiF and CaF_2:Mn, the CaF_2:Mn TLDs display better linearity (higher correlation) and smaller standard deviations within each TLD subset than the LiF.

8.0 Conclusions

The following conclusions have been drawn as a result of this work. Use of the microprocessor for system control gave good reproducibility and made the system more versatile with the availability of its RAM memory for entering new programs. The most significant hardware problems were not found in the control circuitry but in the comparator circuits of its Harshaw and PAR units which exhibited instability and oscillation problems.

When optimizing the system's high voltage and discriminator levels it is important to use the correct form of the SNR given in Eq. (5-1) with the experimental rather that the Poisson standard deviation. Use of these optimizing criteria gave not only the best SNR but also resulted in the best system stability. Optimizing the temperature window was not as advantageous because the optimum window is dose dependent.

Washing the TLDs in acidic methanol proved to be very beneficial in improving the system's accuracy at low doses. Background exposures at two hour intervals (approximately 15.6 μrad intervals) were clearly distinguishable and showed good linearity. The upper limit of the system is characterized by a PMT dead time of 13.0 ns which causes a lose of linearty at a dose of approximately 50 rad. Use of a neutral density filter, however, extended the linear range of the system to 3000 rad for a filter with optical density of 2.0. A filter with higher optical density could extend the range even further.

Finally, the photon counting system performed much better at low doses than the commercial DC system which was virtually useless for doses below approximately 0.5 mrad.

9.0 Suggestions for Further Study

As a result of the investigations reported here, ideas for further research have emerged.

The selection of TLD heating rate reported in Section 5.5 was based on the results reported for only two different rates. To select a truly optimum value many more heating rates should be tested. More research is also needed concerning the acidic methanol wash to determine if it reduces TLD sensitivity with repeated use.

To examine the photon counting system's usefullness in more industrial-like situations, experiments should be performed without the oven annealing processes because most TLD personnel dosimetry is done without annealing. It might also be pertinent to check the system's performance when used in TLD neutron dosimetry and with other TLD materials. And, as a possible means of increasing low dose effectiveness, the ultraviolet sensitization procedure reported in Section 2.4 should be investigated.

10.0 Acknowledgements

I would first like to convey my appreciation to Dr. G. G. Simons for his guidance and counsel as the research was performed and for his help in reviewing and preparing this thesis. I am also grateful to the Department of Nuclear Engineering for financial support provided.

In addition, thanks go to my wife, Amy, and my parents, Ken and Bobbie Harms, for providing this opportunity and offering their continual support and encouragement.

11.0 References

1. K.Z. Morgan and J.E. Turner, Principles of Radiation Protection, Krieger Publ. Co., Huntington, New York (1973).

2. Yigal S. Horowitz and John Kalef-Ezra, "Relative Thermoluminescent Yield of Heavy Charged Particles: Theory and Experiment," Nucl. Instr. and Meth. 175, 29 (1980).

3. Klaus Hübner, Jürgen Henniger, and Dieter Negwer, "LET Dependance of the TL Response and Range Measurements of Heavy Charged Particles in TL Detectors," Nucl. Instr. and Meth. 175, 34 (1980).

4. J. Fain, M. Montret, and L. Sahraoui, "Thermoluminescent Response of CaF_2:Dy and LiF:Mg, Ti Under Heavy Ion Bombardment," Nucl. Instr. and Meth. 175, 37 (1980).

5. J.W.N. Tuyn, "Response of LiF(TLD-700) Thermoluminescence Detectors to Pions and High Energy Neutrons," Nucl. Instr. and Meth. 175, 40 (1980).

6. K.K. Shvarts, F.A. Grant, E.A. Nemiro, M.M. Grube, and D. J. Gubatova, "Physical Principles of Thermoluminescent Dosimetry and Parameters of the Applied Detectors," Fourth Int. Conf. Lum. Dos., Krakow-Poland, 1 (1974).

7. J.B. Lasky, D.W. Pearson, and P.R. Moran, "A Photon Counting System for Thermoluminescent Dosimetry," USAEC Report COO-1105-188 (1973).

8. T. Niewiadomski, "Determination of Optimum Conditions for Photon Counting in Thermoluminescence Measurements," IAEA-SM-160, 199 (1972).

9. Donald W. Hanna, "Development and Optimization of a Thermoluminescent Dosimeter (TLD) Analyzer System for Low-Dose Measurements Utilizing Photon Counting Techniques," Master's Thesis, Kansas State Univ. (1979).

10. A.F. McKinlay, Thermoluminescence Dosimetry, Adam Hilger Ltd., Bristol-England, (1981).

11 C.M.H. Driscoll and A.F. McKinlay, "Factors Affecting the Background Sensitivity of Thermoluminescent Lithium Floride," Nucl. Instr. and Meth. 175, 65 (1980).

12. Hans-Jorg Kos and Reinhard Nink, "Lithium Flouride Dosimetry," Nucl. Instr. and Meth. 175, 24 (1980).

13. M.W. Charles, H.D. Mistry, and Z.U. Khan, "The Theory and Practice of Simultaneous Sensitization and Re-estimation in Lithium Flouride," Nucl. Instr. and Meth. 175, 51 (1980).

14. A.R. Jones, "The Application of Sensitized Lithium Flouride TLDs to Personnel and Environmental Dosimetry," Nucl. Inst. and Meth. 175, 145 (1980).

15. Wilfried Wachter, Norbert J. Vana, and Hannes Aiginger, "The Influence of Hydroxyl Ions on the Thermoluminescence Properties of LiF:Mg, Ti," Nucl. Instr. and Meth. 175, 21 (1980).

16. Gail de Planque, Henri W. Julius, and Cees W. Verhoef, "Effects of Storage Intervals on the Sensitivity and Fading of LiF TLDs," Nucl. Instr. and Meth. 175, 177 (1980).

17. Toshiyuki Nakajima, "Theoretical Considerations of Thermoluminescence Response," J. Appl. Phys. 48, 4880 (1977).

18. RCA Photomultiplier Manual, RCA Electronic Components, U.S.A. (1970).

19. J.R. Prescott, Nucl. Instr. and Meth. 39, 173 (1966).

20. Per Spanne, "Comparison of Photon Counting and Charge Integration as Signal Registration Methods in Low Dose TL Measurements," Fourth Int. Conf. Lum. Dos., Krakow-Poland (1974).

21. A.A. Cafolla, J. N. Carter, C.F.G. Delaney, and I.R. McDonald, "A Computation on Secondary Electron Emission Statistics and its Application to Single Electron Spectra in Photo-and Electron Multipliers," Nucl. Instr. and Meth. 128, 157 (1975).

22. Mikio Yamashita, "Time Dependence of Rate-Dependent Photomultiplier Gain and its Implications," Rev. Sci. Instr. 51, 768 (1980).

23. J.K. Nakamura and S.E. Schwarz, "Synchronous Detection vs. Pulse Counting for Sensitive Photomultiplier Detection Systems," Appl. Optics 7, 1073 (1968).

24. Y.D. Harker, J.D. Masso, and D.F. Edwards, Appl. Optics 8, 2563 (1969).

25. A.T. Young, "Photometric Error Analysis. IX: Optimum Use of Photomultipliers," Appl. Optics 8, 2431 (1969).

26. A.T. Young, "Cosmic Ray Induced Dark Current in Photomultiplier Tubes," Rev. Sci. Instr. 37, (1966).

27. P. Horowitz and W. Hill, The Art of Electronics, Cambridge University Press, U.S.A. (1980).

28. Richard A. Borders, John W. Birks, and John A. Borders," High Speed Pulse Amplifier/Discriminator and Counter for Photon Counting," Anal. Chem. 52, 1273 (1980).

29. R. Jones, C.J. Oliver, and E.R. Pike, "Experimental and Theoretical Comparison of Photon-Counting and Current Measurements of Light Intensity," Appl. Optics 10, 1673 (1971).

30. J.D. Ingle, Jr., and S.R. Crouch, "Critical Comparison of Photon Counting and Direct Current Measurement Techniques for Quantitative Spectrometric Methods," Anal. Chem. 44. 785 (1972).

31. F. Robben, "Noise in the Measurement of Light with Photomultipliers," Appl. Optics 10, 776 (1971).

32. J. Rolfe and S.E. Moore, "The Efficient Use of Photomultiplier Tubes for Recording Spectra," Appl. Optics 9, 63 (1970).

33. C. Nollmann, B. Burgkhardt and E. Piesch, "Parameters Affecting the Overall Calibration Accuracy in TLD 700 Thermoluminescence Dosimetry," Nucl. Instr. and Meth. 161, 449 (1979).

34. Model 1121 Amplifier-Discriminator Operating and Service Manual, Princeton Applied Research, U.S.A. (1976)

35. Model 1109 Photon Counter Operating and Service Manual, Princeton Applied Research, U.S.A. (1976).

36. E.J. Darland, J.E. Hornshuh, C.G. Enke, and G.E. Leroi, "Pulse (Photon) Counting: A High-Speed, Direct Current-Coupled pulse Counter," Anal. Chem. 51, 245 (1979).

37. W.L. Reiter and G. Stengl, "A Long Term Stable Reference Light Source Using LEDs for Stabilization of Scintillation Spectrometers," Nucl. Instr. and Meth. 173, 275 (1980).

38. W.L. Reiter and G. Stengl, "A Blue Light Emitting Diode Used as a Reference Element in Scintillation Spectrometers," Nucl. Instr. and Meth. 180, 105 (1981).

39. E.J. Darland, G.E. Leroi, and C.G. Enke, "Maximum Efficiency Pulse Counting in Computerized Instrumentation," Anal. Chem. 52, 714 (1980).

40. G.A. Morton, "Photon Counting," Appl. Optics 7, 1 (1968).

41. T.M. Niemczyk, D.G. Ehinger, and S.G. Barnhart," Optimization of Parameters in Photon Counting Experiments," Anal. Chem. 51, 2001 (1979).

42. J.D. Ingle, Jr., and S.P. Crouch, "Pulse Overlap Effects on Linearity and Signal-to-Noise Ratio in Photon Counting Systems," Anal. Chem. 44, 777 (1973).

43. Robert M. Ostmeyer, "^{7}LiF and CaF_2:Mn Experimental Data for Evaluating TLD Energy Response Theory," Master's Thesis, Kansas State Univ. (1980).

44. F.M. Cox, A.C. Lucas, and B.M. Kapsar, "The Reusability of Solid Thermoluminescent Dosimeters and its Relation to the Maintenance of TL Standards," Health Physics 30, 135 (1976).

45. P. Spanne, Acta Radiologica, Suppl. 360 (1979).

46. T. Schlesinger, A. Avni, Y. Feige, and S.S. Friedland, "Photon Counting as Applied to Thermoluminescence Dosimetry," Riso Report 249 (Danish Atomic Energy Commission Establishment, Riso), 226 (1971).

47. Glenn F. Knoll, Radiation Detection and Measurement, John Wiley & Sons, New York (1979).

Appendix A. Microprocessor Program MOVE

This program will transfer the program PC CONTROL
from EPROM ($C000) to RAM ($0000).

It should be entered at $0130.

See Appendix D for further instructions.

ADDRESS	MACHINE CODE			LABEL	MNEMONICS			COMMENTS
0130	CE	00	00		LDX	#	$0000	
0133	FF	01	D2		STX		$01D2	SET RAM POINTER
0136	CE	C0	00		LDX	#	$C000	
0139	A6	00		LOOP	LDAA		0,X	GET ROM DATA
013B	FF	01	D0		STX		$01D0	STORE ROM POINTER
013E	FE	01	D2		LDX		$01D2	RETRIEVE RAM POINTER
0141	A7	00			STAA		0,X	STORE DATA IN RAM
0143	08				INCX			
0144	FF	01	D2		STX		$01D2	INCREMENT & STORE RAM POINTER
0147	FE	01	D0		LDX		$01D0	RETRIEVE & INCREMENT ROM POINTER
014A	08				INCX			
014B	8C	C1	2E		CPX	#	$C12E	DONE ?
014E	26	E9			BNE		LOOP	IF NOT, REPEAT
0150	3F				SWI			

Appendix B. Flowchart of Microprocessor Program PC CONTROL

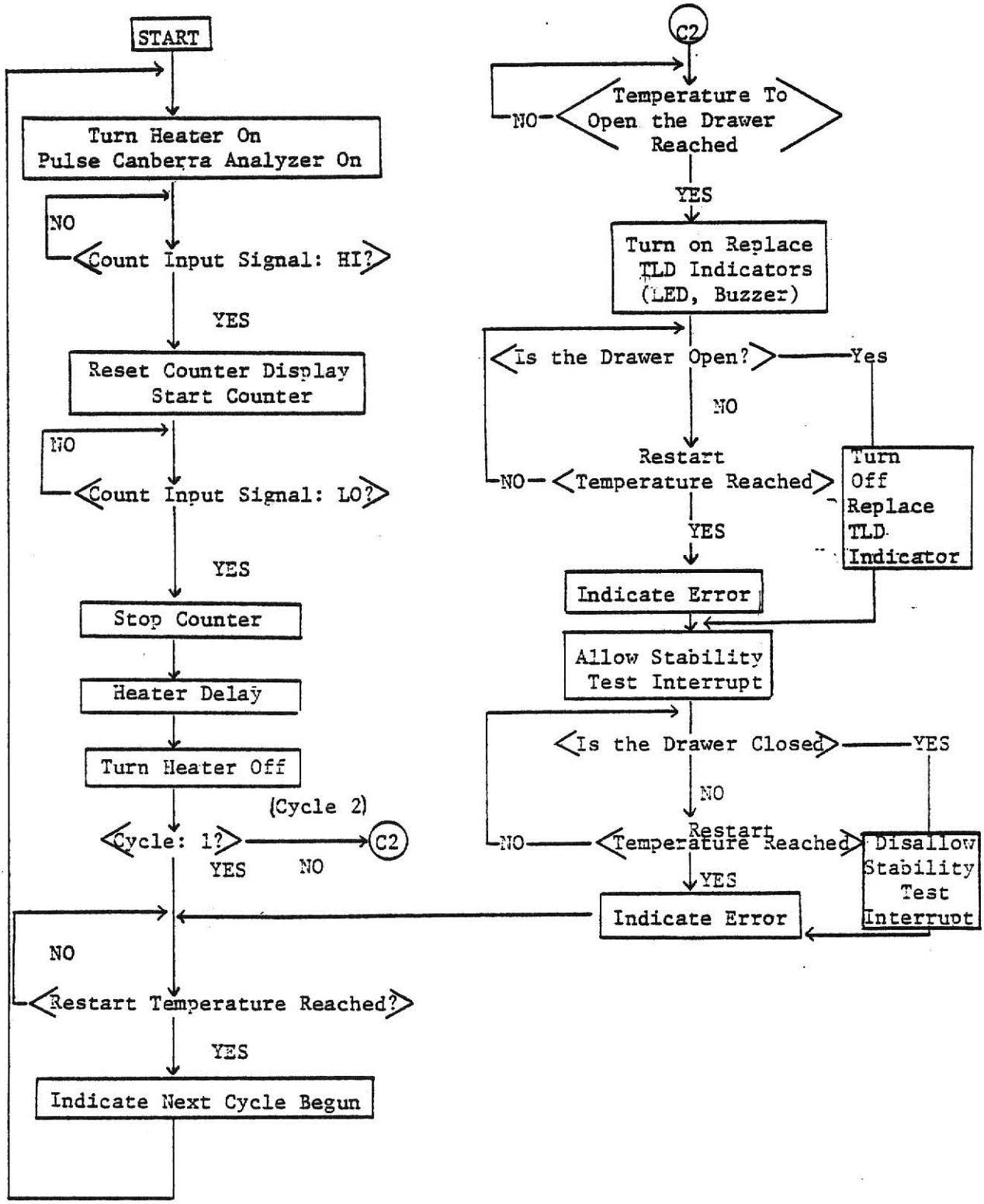

Appendix C. Microprocessor Program PC CONTROL

ADDRESS	MACHINE CODE			LABEL	MNEMONICS		COMMENTS
					RESET PROGRAM		
C000	CE	C1	00		LDX	# $0100	
C003	FF	A0	00		STX	$A000	SET INTERRUPT VECTOR
C006	CE	80	04		LDX	# $8004	
C009	6F	01			CLR	1,X	POINT TO DDRs
C00B	6F	03			CLR	3,X	
C00D	86	F0			LDAA	# $F0	A0-A3 INPUTS
C00F	87	00			STAA	0,X	
C011	86	FF			LDAA	# $FF	B0-B6 OUTPUTS
C013	A7	02			STAA	2,X	
C015	86	2D			LDAA	# % 0010 1101	CA2 NOT USED, CAI INT. ON H TO L
C017	87	01			STAA	1,X	
C019	86	3C			LDAA	# % 0011 1100	CB1, CB2 NOT USED
C01B	A7	03			STAA	3,X	
C01D	86	80			LDAA	# $80	SET B0-B6 LOW, B7 HI
C01F	A7	02			STAA	2,X	
C021	E6	00			LDAB	0,X	CLEAR IRQ 7
C023	3F				SWI		
					LED TEST		
C030	0E			TEST	CLI		HERE FOR INITIAL LED TEST
C031	3E				WAI		
C032	A6	02			LDAA	2,X	
C034	84	DF			ANDA	# % 1101 1111	TURN OFF ERROR LIGHT
C036	A7	02			STAA	2,X	
C038	20	F6			BRA	TEST	
					MAIN PROGRAM		
C040	0F				SEI		HERE TO BEGIN CYCLE
C041	A6	02		START	LDAA	2,X	
C043	8A	44			ORAA	# % 0100 0100	SET READ, CANBERRA HI
C045	A7	02			STAA	2,X	
C047	CE	FF	FF		LDX	# $FFFF	
C04A	BD	E0	E0		JSR	$E0E0	DELAY 0.85 SEC. (REQUIRED
C04D	CE	80	04		LDX	# $8004	BY CANBERRA INPUT)
C050	84	BF			ANDA	# % 1011 1111	SET CANBERRA LO
C052	A7	02			STAA	2,X	
C054	E6	00		LOOP 1	LDAB	0,X	TEST FOR INTEGRATE HI
C056	C4	01			ANDB	# % 0000 0001	
C058	27	FA			BEQ	LOOP 1	
C05A	84	7F			ANDA	# % 0111 1111	WHEN INTEGRATE IS HI,
C05C	A7	02			STAA	2,X	PULSE RESET/START LO,
C05E	8A	80			ORAA	# % 1000 0000	
C060	A7	02			STAA	2,X	BACK HI
C062	8A	08			ORAA	# % 0000 1000	
C064	A7	02			STAA	2,X	SET HOLD HI (START COUNTING)

ADDRESS	MACHINE CODE			LABEL	MNEMONIC		COMMENTS
C066	F6	01	FD		LDAB	$01FD	DELAY TO "DEBOUNCE" COUNT SIGNAL
C069	BD	C0	D0		JSR	DELAY	
C06C	E6	00		LOOP 2	LDAB	0,X	
C06E	C4	01			ANDB	# % 0000 0001	TEST FOR INTEGRATE LOW
C070	26	FA			BNE	LOOP 2	CONTINUE WHEN IT IS
C072	84	F7			ANDA	# % 1111 0111	
C074	A7	02			STAA	2,X	SET HOLD LOW (STOP COUNTING)
C076	F6	01	FF		LDAB	$ 01FF	GET # OF ½ SECS. FOR DELAY
C079	BD	C0	D0		JSR	DELAY	
C07C	84	DB			ANDA	# % 1101 1011	SET READ LOW, TURN OFF ERROR
C07E	A7	02			STAA	2,X	
C080	E6	02			LDAB	2,X	
C082	C4	10			ANDB	# % 0001 0000	IF CYCLE 1, JUMP TO LOOP 6
C084	27	34			BEQ	LOOP 6	
C086	E6	00		LOOP 3	LDAB	0,X	
C088	C4	02			ANDB	# % 0000 0010	TIME TO OPEN DRAWER?
C08A	26	FA			BNE	LOOP 3	
C08C	8A	01			ORAA	# % 0000 0001	SIGNAL TO OPEN DRAWER
C08E	A7	02			STAA	2,X	
C090	E6	00			LDAB	0,X	
C092	C4	08			ANDB	# % 0000 1000	DRAWER OPEN?
C094	26	0C			BNE	CLOSE	IF SO, GO TO CLOSE
C096	E6	00			LDAB	0,X	
C098	C4	04			ANDB	# % 0000 0100	COOLED TO RESTART TEMP. YET?
C09A	26	F4			BNE	LOOP 4	IF NOT, LOOP BACK
C09C	8A	20			ORAA	# % 0010 0000	IF SO, LIGHT ERROR LIGHT
C09E	A7	02			STAA	2,X	AND WAIT FOR DRAWER TO OPEN
C0A0	20	EE			BRA	LOOP 4	
C0A2	84	FE		CLOSE	ANDA	# % 1111 1110	TURN OFF REPLACE INDICATORS
C0A4	A7	02			STAA	2,X	
C0A6	0E				CLI		ENABLE LED TEST
C0A7	E6	00		LOOP 5	LDAB	0,X	
C0A9	C4	08			ANDB	# % 0000 1000	DRAWER CLOSED?
C0AB	27	0C			BEQ	RESTART	IF SO GO TO RESTART
C0AD	E6	00			LDAB	0,X	
C0AF	C4	04			ANDB	# % 0000 0100	COOLED TO RESTART TEMP. YET?
C0B1	26	F4			BNE	LOOP 5	IF NOT LOOP BACK
C0B3	8A	20			ORRA	# % 0010 0000	IF SO LIGHT ERROR LIGHT
C0B5	A7	02			STAA	2,X	AND WAIT FOR DRAWER TO CLOSE
C0B7	20	EE			BRA	LOOP 5	
C0B9	0F			RESTART	SEI		DISABLE LED TEST

ADDRESS	MACHINE CODE			LABEL	MNEMONICS		COMMENTS
C0BA	E6	00		LOOP 6	LDAB	0,X	
C0BC	C4	04			ANDB # % 0000 0100		COOLED TO RESTART TEMP YET?
C0BE	26	FA			BNE	LOOP 6	WAIT FOR RESTART TEMP.
C0C0	88	10			EORA # % 0001 0000		
C0C2	A7	02			STAA	2,X	TOGGLE CYCLE BIT
C0C4	7E	C0	41		JMP	START	
				INTERRUPT PROGRAM			
C100	CE	80	04		LDX # % 8004		
C103	A6	02			LDAA	2,X	
C105	8A	02			ORAA # % 0000 0010		TURN TEST LED ON
C107	A7	02			STAA	2,X	
C109	84	7F			ANDA # % 0111 1111		PULSE RESET/START
C10B	A7	02			STAA	2,X	LOW,
C10D	8A	80			ORAA # % 1000 0000		
C10F	A7	02			STAA	2,X	THEN HI
C111	8A	08			ORAA # % 0000 1000		HOLD GOES HI (START COUNTING)
C113	A7	02			STAA	2,X	
C115	F6	01	FE		LDAB	$01FE	GET # OF ½ SECS. FOR DELAY
C118	BD	C0	D0		JSR	DELAY	DELAY
C11B	84	F7			ANDA # % 1111 0111		SET HOLD LOW (STOP COUNTING)
C11D	A7	02			STAA	2,X	
C11F	84	FD			ANDA # % 1111 1101		TURN OFF TEST LED
C121	A7	02			STAA	2,X	
C123	E6	00			LDAB	0,X	
C125	C4	04			ANDB # % 0000 0100		COOLED TO RESTART TEMP. YET?
C127	26	04			BNE	RETURN	
C129	8A	20			ORAA # % 0010 0000		IF SO, INDICATE ERROR
C12B	A7	02			STAA	2,X	
C12D	3B			RETURN	RTI		
				DELAY SUBROUTINE			
C0D0	CE	96	00	LOOP 7	LDX # % 9600		SET X FOR ½ SEC. LOOPS
C0D3	09			LOOP 8	DECX		
C0D4	26	FD			BNE	LOOP 8	
C0D6	5A				DECB		
C0D7	26	F7			BNE	LOOP 7	
C0D9	CE	80	04		LDX # $ 8004		RESTORE POINTER
C0DC	39				RTS		

IMPORTANT LOCATIONS

A0000	0100		INTERRUPT VECTOR (PRESET)
01FD	(10) NOMINAL		COUNT SIGNAL "DEBOUNCE"
01FE	(10) NOMINAL	}DELAYS IN $ ½ SECS.	TEST LED
01FF	(20) NOMINAL		HEAT AFTER T_2

Appendix D. Operator's Manual

Appendix C contains a listing of the version of PC CONTROL in the EPROM. This program has an error at location C001 where 01 should be C1. This problem may be overcome by manually storing C1 in location A000 and 00 in location A001. Then instead of starting the reset program at C000 start at C006.

This version of PC CONTROL also cycles each TLD through the readout process twice. The easiest way to make this and other alterations is to use the program MOVE in Appendix A to transfer the program from EPROM (C000) to RAM (0000). MOVE should be entered at location 0130. Once the program is in RAM the following changes must be made.

ADDRESS	OLD CONTENTS	NEW CONTENTS
006A	C0	00
007A	C0	00
00C5	C0	00
0119	C0	00

Now the program may be modified as desired. For instance, to cycle each TLD through only one readout cycle make the following change:

ADDRESS	OLD CONTENTS	NEW CONTENTS
0084	27	20

Initialization

These instructions assume that PC CONTROL has been transferred to location 0000.

Turn on the Motorola power supply.

Key in 0000 and press G. 0023 3F should appear on the display.

Turn readout unit power on.

Flip counter power switch and amplifier/discriminator power switch to "on". (Switchs will light up)

Turn the high voltage up to the desired level (2120 V Nominally). The power switch on the high voltage unit should always be left in the "on" position.

Set T_1 (counter start temperature) and T_2 (counter stop temperature) to the desired levels. Suggested values: 130°C-200°C for LiF, 150°C-250°C for CaF_2:Mn.

Set $T_{restart}$ and $T_{replace}$ to the nominal values marked on the dial and adjust as needed.

Select the heating profile appropriate for the type of TLD being used.

Determine the delay desired from T_2 until the heat turns off.

Determine the number of 1/2 seconds in the delay and convert this to a hexadecimal (base 16) number.

Hit E.

Key in 01FF and then the two digit number calculated above.

Determine the length of time desired for the test LED count.

Convert this number to 1/2 seconds in hexadecimal as above.

Hit E.

Key in 01FE and then the two digit number calculated above.

Determine the length of time needed to debounce the integrate signal (6.5 sec. nominally).

Convert to 1/2 seconds in hexadecimal.

Hit E.

Key in 01FD and then the two digit number calculated above.

<u>To Check the Test LED:</u>

Hit E.

Key in 0030 G.

When the test button is pushed the test LED will be lit and the counter will reset and count for the time specified by the number in 01FE. When the indicator light goes off the button may be pushed again to repeat the cycle as often as desired.

When testing is completed, hit E, and then 0000 G.

Note: The error light may come on during the test but it has no meaning in this mode of operation.

Using the MCA

The power switch on the MCA should be left on at all times.

If the MCA is being used it should be programmed to execute the following task:

PAUSE
COLLECT
READOUT
CLEAR DATA
GO TO 1

The dwell time should be set so that the number of channels multiplied by the dwell time is approximately equal to the length of the heat cycle. For example, with 1024 channels 40 msec. may be an appropriate dwell time.

When the analyzer is properly configured, execute the task.

For more information on operating the analyzer see the MCA operators manual.

General Operation

To begin the readout cycle key in 0040 G.

Note: Let the system cycle several times before reading out any TLDs.

When ready to read out a TLD, wait for buzzer to sound. Then open the drawer, put in a TLD and close the drawer. The cycle will restart and the counter will record the first reading. The process will be repeated. This time the number on the counter should be recorded as background. When the buzzer sounds open the drawer, replace the TLD and repeat the process. (If the program has been modified to cycle each TLD only once, follow instructions for cycle 2 each cycle.) If the drawer is not closed before the heater cools to the restart temperature the error light will come on. If this happens continue the readout process as before, but indicate that the data may be inaccurate.

When finished reading out all TLDs;

Hit E.

Key in 0000 G.

Equipment should be turned off in the following order:

Turn high voltage to 0V
Turn off discriminator
Turn off counter
Turn off heater
Turn off Motorola power supply.

Special Operation

Adjusting the temperature profile:

Key in 0000 G.

Hit E.

Key in 8006 M 04. This turns on the heater.

Key in 00 to turn off the heater.

Any of the instruments controlled by the microprocessor or the corresponding LEDs on the display may be checked by keying in 8006 M and the appropriate number from the list below.

Cycle 1	00
Cycle 2	10
Heat	04
Count	08
Test LED	02
Error	20
Replace Indicators	01
Reset Counter	80
Start MCA	40
Drawer Open	Open the drawer

When any special operations are completed hit E, and then;

Key in 0000 G.

Appendix E. Fortran Program OPTPC

```
C***   PROGRAM: OPTPC
C***   PROGRAMMER: BRIAN HARMS   6/81
C*   THIS PROGRAM FINDS THE OPTIMUM UPPER AND LOWER DISCRIMINATOR LEVELS FOR A
C*   PHOTON COUNTING SYSTEM BASED ON EACH OF THE FOLLOWING PERFORMANCE MEASURES:
C*            SIGNAL/NOISE
C*            SIGNAL/NOISE  EXPERIMENTAL
C*            TOTAL/DARK
C*            SIGNAL/DARK
C*            TOTAL/NOISE-IN-DARK
C*            TOTAL/NOISE-IN-DARK  EXPERIMENTAL
C*            SIGNAL/NOISE-IN-DARK
C*            SIGNAL/NOISE-IN-DARK EXPERIMENTAL
C*   USING THE EQUATIONS FOLLOWING STATEMENT 25.
C*
C*   TINTM AND DINTM ARE THE MEAN INTEGRAL PULSE HEIGHT DISTRIBUTIONS (PHD) FOR
C*   TOTAL AND DARK, RESPECTIVELY, CALCULATED FROM THE N INPUT DIFFERENTIAL PHDS.
C*   TINVAR AND DINVAR ARE THE CORRESPONDING EXPERIMENTAL VARIANCES.
C*
C*   POISSON STATISTICS ARE ASSUMED FOR THE NON-EXPERIMENTAL RATIOS
C*   I.E. VARIANCE=MEAN.
C*
C*
C*** INPUT
C*            SPECTRA FROM THE SERIES 90 MCA RECORDED ON MAG TAPE
C*            256 CHANNELS/SPECTRUM, BCD ENCODED
C*            1 CARD IN MAIN DECK: N= NUMBER OF 'TOTAL' SPECTRA (ALSO EQUAL TO
C*            THE NUMBER OF DARK SPECTRA).
C*
C*
C*** OUTPUT
C*            1-THE VARIOUS PERFORMANCE MEASURES DESCRIBED ABOVE AS A FUNCTION OF
C*              LOWER LEVEL DISC. (LLD).
C*            2-COMPARISON OF POISSON AND EXPERIMENTAL STANDARD DEVIATIONS.
C*            3-THE VARIOUS PERFORMANCE MEASURES DESCRIBED ABOVE AS A FUNCTION OF
C*              UPPER LEVEL DISC. (ULD) USING THE LLD SETTING GIVEN AS OPTIMUM
C*              IN 1 ABOVE.
C*
C*
      DIMENSION TINT(257,10),DINT(257,10),TINTM(256),DINTM(256)
      DIMENSION TINVAR(256),DINVAR(256),TOTAL(256,10),DARK(256,10)
      DIMENSION SNU(256),SNEXU(256),TOU(256),SOU(256),TNOU(256)
      DIMENSION TNOEXU(256),SNOU(256),SNOEXU(256)
      INTEGER TOTAL,DARK,TINT,DINT,USN,USNEX,UTO,USO,UTNO,UTNOEX,USNO
      INTEGER USNOEX
      INTEGER CUSN,CUSNEX,CUTO,CUSO,CUTNO,CUTNOE,CUSNO,CUSNOE
      INTEGER CLSN,CLSNEX,CLTO,CLSO,CLTNO,CLTNOE,CLSNO,CLSNOE
C
  200 FORMAT(' ')
  206 FORMAT('1',18X,'TOTAL COUNT')
  207 FORMAT('1',18X,'DARK COUNT')
  210 FORMAT(' CHANNEL      POISSON STANDARD DEV.      EXPERIMENTAL STANDA
     1RD DEV.')
  212 FORMAT(2X,I3,14X,F6.1,23X,F6.1)
  220 FORMAT('1CHANNEL    S/N      S/N EX      T/O      S/O      T/NO     T/
     1NOEX     S/NO    S/NOEX')
  222 FORMAT(2X,I3,5X,8(F6.1,3X))
  223 FORMAT(' RATIO',5X,8(F6.1,3X))
  224 FORMAT(30X,'OPTIMUMS')
```

```
  226 FORMAT(' CHANNEL',3X,8(2X,I3,4X))
  298 FORMAT(I6,(T7,16(16I6)))
  502 FORMAT('1  ERROR IN DATA ENCOUNTERED - JOB ABANDONNED')
  503 FORMAT('   UNEXPECTEDLY RAN OUT OF DATA')
C
C*  READ IN DATA
      N=10
      DO 1 J=1,N
      READ(8,298,END=180,ERR=181)ID,(TOTAL(I,J),I=1,256)
    1 READ(8,298,END=180,ERR=181)ID,(DARK(I,J),I=1,256)
      DSN=0
      DSNEX=0
      DTD=0
      DSD=0
      DTNO=0
      DTNDEX=0
      DSNO=0
      DSNDEX=0
C
      DO 10 I=1,257
      DO 9 J=1,N
      TINT(I,J)=0
    9 DINT(I,J)=0
   10 CONTINUE
      WRITE(6,200)
      WRITE(6,200)
      WRITE(6,220)
C
C*  CALCULATE INDIVIDUAL INTEGRAL PHOS AND FIND MEAN
      DO 50 K=1,254
      I=256-K+1
      DO15 J=1,N
      TINT(I,J)=TINT(I+1,J)+TOTAL(I,J)
   15 DINT(I,J)=DINT(I+1,J)+DARK(I,J)
      TINTM(I)=0
      DINTM(I)=0
      DO 20 J=1,N
      TINTM(I)=TINTM(I)+TINT(I,J)
   20 DINTM(I)=DINTM(I)+DINT(I,J)
      TINTM(I)=TINTM(I)/N
      DINTM(I)=DINTM(I)/N
C
C*  CALCULATE VARIANCE OF INTEGRAL PHOS
      TINVAR(I)=0
      DINVAR(I)=0
      DO 25 J=1,N
      TINVAR(I)=TINVAR(I)+(TINTM(I)-TINT(I,J))**2
   25 DINVAR(I)=DINVAR(I)+(DINTM(I)-DINT(I,J))**2
      TINVAR(I)=TINVAR(I)/(N-1)
      DINVAR(I)=DINVAR(I)/(N-1)
C
C*  CALCULATE PERFORMANCE MEASURES AS A FUNCTION OF LLD, AND FIND OPTIMUMS
      SN=(TINTM(I)-DINTM(I))/SQRT(TINTM(I)+DINTM(I))
      SNEX=(TINTM(I)-DINTM(I))/SQRT(TINVAR(I)+DINVAR(I))
      TD=TINTM(I)/DINTM(I)
      SD=(TINTM(I)-DINTM(I))/DINTM(I)
      TNO=TINTM(I)/SQRT(DINTM(I))
      TNDEX=TINTM(I)/SQRT(DINVAR(I))
```

```
      SND=(TINTM(I)-DINTM(I))/SQRT(DINTM(I))
      SNDEX=(TINTM(I)-DINTM(I))/SQRT(DINVAR(I))
      IF(SN.GT.CSN)LSN=I
      IF(SNEX.GT.CSNEX)LSNEX=I
      IF(TD.GT.CTD)LTD=I
      IF(SD.GT.CSD)LSD=I
      IF(TND.GT.CTND)LTND=I
      IF (TNDEX.GT.CTNDEX)LTNDEX=I
      IF(SND.GT.CSND)LSND=I
      IF(SNDEX.GT.CSNDEX)LSNDEX=I
      DSN=AMAX1(DSN,SN)
      DSNEX=AMAX1(DSNEX,SNEX)
      DTD=AMAX1(TD,CTD)
      DSD=AMAX1(SD,DSD)
      DTND=AMAX1(TND,DTND)
      DTNDEX=AMAX1(DTNDEX,TNDEX)
      DSND=AMAX1(SND,DSND)
      DSNDEX=AMAX1(SNDEX,DSNDEX)
      ICHAN=I-1
C
C*  OUTPUT 1
   50 WRITE(6,222)ICHAN,SN,SNEX,TD,SD,TND,TNDEX,SND,SNDEX
      WRITE(6,224)
      WRITE(6,223)DSN,DSNEX,DTD,DSD,DTND,DTNDEX,DSND,DSNDEX
      CLSN=LSN-1
      CLSNEX=LSNEX-1
      CLTD=LTD-1
      CLSD=LSD-1
      CLTND=LTND-1
      CLTNDE=LTNDEX-1
      CLSND=LSND-1
      CLSNDE=LSNDEX-1
      WRITE(6,226)CLSN,CLSNEX,CLTD,CLSD,CLTND,CLTNDE,CLSND,CLSNDE
      WRITE(6,200)
      WRITE(6,200)
      WRITE(6,206)
      WRITE(6,200)
      WRITE(6,210)
C
C*  CALCULATE POISSON AND EXPERIMENTAL STANDARD DEVIATIONS
C*  OUTPUT 2
      DO 60 I=3,256
      POISS=SQRT(TINTM(I))
      EXP=SQRT(TINVAR(I))
      ICHAN=I-1
   60 WRITE(6,212)ICHAN,POISS,EXP
      WRITE(6,200)
      WRITE(6,200)
      WRITE(6,207)
      WRITE(6,200)
      WRITE(6,210)
      DO 70 I=3,256
      POISS=SQRT(DINTM(I))
      EXP=SQRT(DINVAR(I))
      ICHAN=I-1
   70 WRITE(6,212)ICHAN,POISS,EXP
C
      DSN=0
```

```
      OSNEX=0
      OTD=0
      OSD=0
      OTND=0
      OTNDEX=0
      OSNO=0
      OSNOEX=0
      DO 75 I=1,256
      SNU(I)=0
      SNEXU(I)=0
      TDU(I)=0
      SDU(I)=0
      TNDU(I)=0
      TNDEXU(I)=0
      SNDU(I)=0
   75 SNDEXU(I)=0
C
C*  CALCULATE PERFORMANCE MEASURES AS A FUNCTION OF ULD WITH OPTIMUM LLD, FIND
C*  OPTIMUMS.
      L=LSN
      IF(L.GT.255)GO TO 80
      CALL GRIND(L,N,TINT,OINT,TOTAL,DARK,TINTM,OINTM,TINVAR,OINVAR)
      DO 77 I=L,256
      SNU(I)=(TINTM(I)-OINTM(I))/SQRT(TINTM(I)+OINTM(I))
      IF(SNU(I).GT.OSN)USN=I
   77 OSN=AMAX1(SNU(I),OSN)
   80 CONTINUE
C
      L=LSNEX
      IF(L.GT.255)GO TO 90
      CALL GRIND(L,N,TINT,OINT,TOTAL,DARK,TINTM,OINTM,TINVAR,OINVAR)
      DO 85 I=L,256
      SNEXU(I)=(TINTM(I)-OINTM(I))/SQRT(TINVAR(I)+OINVAR(I))
      IF(SNEXU(I).GT.OSNEX)USNEX=I
   85 OSNEX=AMAX1(SNEXU(I),OSNEX)
   90 CONTINUE
C
      L=LTD
      IF(L.GT.255)GO TO 100
      CALL GRIND(L,N,TINT,OINT,TOTAL,DARK,TINTM,OINTM,TINVAR,OINVAR)
      DO 95 I=L,256
      TDU(I)=TINTM(I)/OINTM(I)
      IF(TDU(I).GT.OTD)UTD=I
   95 OTD=AMAX1(TDU(I),OTD)
  100 CONTINUE
C
      L=LSD
      IF(L.GT.255)GO TO 110
      CALL GRIND(L,N,TINT,OINT,TOTAL,DARK,TINTM,OINTM,TINVAR,OINVAR)
      DO 105 I=L,256
      SDU(I)=(TINTM(I)-OINTM(I))/OINTM(I)
      IF(SDU(I).GT.OSD)USD=I
  105 OSD=AMAX1(SDU(I),OSD)
  110 CONTINUE
C
      L=LTND
      IF(L.GT.255)GO TO 120
      CALL GRIND(L,N,TINT,OINT,TOTAL,DARK,TINTM,OINTM,TINVAR,OINVAR)
```

```
      DO 115 I=L,256
      TNDU(I)=TINTM(I)/SQRT(DINTM(I))
      IF(TNDU(I).GT.DTND)UTND=I
  115 DTND=AMAX1(TNDU(I),CTND)
  120 CONTINUE
C
      L=LTNDEX
      IF(L.GT.255)GO TO 130
      CALL GRIND(L,N,TINT,DINT,TOTAL,DARK,TINTM,DINTM,TINVAR,DINVAR)
      DO 125 I=L,256
      TNDEXU(I)=TINTM(I)/SQRT(DINVAR(I))
      IF(TNDEXU(I).GT.DTNDEX)UTNDEX=I
  125 DTNDEX=AMAX1(TNDEXU(I),GTNDEX)
  130 CONTINUE
C
      L=LSND
      IF(L.GT.255)GO TO 140
      CALL GRIND(L,N,TINT,DINT,TOTAL,DARK,TINTM,DINTM,TINVAR,DINVAR)
      DO 135 I=L,256
      SNDU(I)=(TINTM(I)-DINTM(I))/SQRT(DINTM(I))
      IF(SNDU(I).GT.CSND)USND=I
  135 DSND=AMAX1(SNDU(I),DSND)
  140 CONTINUE
C
      L=LSNDEX
      IF(L.GT.255)GO TO 150
      CALL GRIND(L,N,TINT,DINT,TOTAL,DARK,TINTM,DINTM,TINVAR,DINVAR)
      DO 145 I=L,256
      SNDEXU(I)=(TINTM(I)-DINTM(I))/SQRT(DINVAR(I))
      IF(SNDEXU(I).GT.CSNDEX)USNDEX=I
  145 DSNDEX=AMAX1(SNDEXU(I),CSNDEX)
  150 CONTINUE
C
C*   OUTPUT 3
      WRITE(6,200)
      WRITE(6,200)
      WRITE(6,200)
      WRITE(6,220)
      DO 160 I=3,256
      ICHAN=I-1
  160 WRITE(6,222)ICHAN,SNU(I),SNEXU(I),TDU(I),SDU(I),TNDU(I),TNDEXU(I),
     1SNDU(I),SNDEXU(I)
      WRITE(6,224)
      WRITE(6,223)DSN,DSNEX,DTD,DSD,CTND,CTNDEX,CSND,CSNDEX
      CUSN=USN-1
      CUSNEX=USNEX-1
      CUTD=UTD-1
      CUSD=USD-1
      CUTND=UTND-1
      CUTNDE=UTNDEX-1
      CUSND=USND-1
      CUSNDE=USNDEX-1
      WRITE(6,226)CUSN,CUSNEX,CUTD,CUSD,CUTND,CUTNDE,CUSND,CUSNDE
      GO TO 175
  180 WRITE(6,503)
      GO TO 175
  181 WRITE(6,502)
  175 CONTINUE
```

```
STOP
END
```

```
C
      SUBROUTINE GRINO(L,N,TINT,OINT,TOTAL,OARK,TINTM,OINTM,TINVAR,OINVAR
     1R)
C*   THIS SUBROUTINE IS USED TO CALCULATE INTEGRAL PHOS WITH A FIXED LLD AND
C*   VARIABLE ULD.
      DIMENSION TINT(257,10),OINT(257,10),TINTM(256),OINTM(256)
      DIMENSION TINVAR(256),OINVAR(256),TOTAL(256,10),OARK(256,10)
      INTEGER TOTAL,OARK,TINT,OINT
      DO 310 I=1,257
      DO 310 J=1,N
      TINT(I,J)=0
  310 OINT(I,J)=0
      L=L+1
      DO 330 I=L,256
      DO 312 J=1,N
      TINT(I,J)=TINT(I-1,J)+TOTAL(I,J)
  312 OINT(I,J)=OINT(I-1,J)+OARK(I,J)
      TINTM(I)=0
      OINTM(I)=0
      DO 314 J=1,N
      TINTM(I)=TINTM(I)+TINT(I,J)
  314 OINTM(I)=OINTM(I)+OINT(I,J)
      TINTM(I)=TINTM(I)/N
      OINTM(I)=OINTM(I)/N
      TINVAR(I)=0
      OINVAR(I)=0
      DO 316 J=1,N
      TINVAR(I)=TINVAR(I)+(TINTM(I)-TINT(I,J))**2
  316 OINVAR(I)=OINVAR(I)+(OINTM(I)-OINT(I,J))**2
      TINVAR(I)=TINVAR(I)/(N-1)
  330 OINVAR(I)=OINVAR(I)/(N-1)
      RETURN
      END
```

Appendix F. Microprocessor Program LED

This program executes 100 second readouts of the LED light source.

ADDRESS	MACHINE CODE		LABEL	MNEMONICS	COMMENTS
0160	CE	80 04		LDX # $ 8004	
0163	A6	02		LDA 2,X	
0165	84	7F	START	ANDA # % 0111 1111	
0167	A7	02		STAA 2,X	PULSE RESET/START LOW,
0169	8A	80		ORAA # % 1000 0000	
016B	A7	02		STAA 2,X	BACK HI
016D	8A	08		ORAA # % 0000 1000	
016F	A7	02		STAA 2,X	SET HOLD HI (COUNT)
0171	C6	CA		LDAB # $ CA	
0173	BD	00 00		JSR DELAY	100 SEC COUNT
0176	84	F7		ANDA # % 1111 0111	
0178	A7	02		STAA 2,X	SET HOLD LO
017A	8A	01		ORAA # % 0000 0001	
017C	A7	02		STAA 2,X	TURN ON BUZZER
017E	C6	04		LDAB # $ 04	
0180	BD	00 DO		JSR DELAY	2 SEC BUZZ
0183	84	FE		ANDA # % 1111 1110	
0185	A7	02		STAA 2,X	TURN OFF BUZZER
0187	C6	10		LDAB # $10	
0189	BD	00 DO		JSR DELAY	WAIT 8 SECS.
018C	20	D7		BRA START	START OVER

THE OPTIMIZATION AND USE OF A PHOTON COUNTING SYSTEM FOR THERMOLUMINESCENT DOSIMETRY

by

BRIAN KENNETH HARMS

B.S., Kansas State University, 1980

AN ABSTRACT OF A MASTER'S THESIS

Submitted in partial fulfillment of the

requirements for the degree

MASTER OF SCIENCE

Department of Nuclear Engineering

KANSAS STATE UNIVERSITY

Manhattan, Kansas

1982

ABSTRACT

A photon counting system for thermoluminescent dosimeter (TLD) analysis was assembled, optimized, and tested to determine its useful range. The system was remotely controlled by a microprocessor to insure good reproducibility of the readout cycles, particularly the restart temperatures. The system's high voltage (HV) and discriminator levels were optimized using the correct expression for signal-to-noise ratio (SNR) and these results were compared to those obtained with other SNRs reported in the literature. The comparison showed that the previously reported SNRs gave very different values of "optimum" HV and discriminator levels. Using these values instead of those corresponding to the correct SNR would result in suboptimal system performance. Using an experimentally determined variance in calculating SNR rather than a Poisson variance was also found to be imperative in accurately determining the optimal discriminator and HV levels. The upper dose limit of the system, due to the 13.0 ns dead time of the photomultiplier tube (PMT), was found to be 50 rads for ^{7}LiF 1x1x6 cm rods (TLD-700). However, by installing a neutral density filter (1.26% transmission at 400 nm) in front of the PMT it was possible to extend the system's upper dose limit to 3000 rad, well beyond the TLD transition to supralinearity. In an effort to improve TLD performance at low doses, a TLD wash using acidic methanol was investigated. The results of the investigation showed that washing the TLDs greatly increased the linearity of their response at low doses. It also decreased the standard deviation obtained within each subset of TLDs receiving the same dose. The photon

counter was compared to a commercial DC TLD analyzer over a dose range of 0.14 to 0.94 mrad using the same ^{7}LiF TLDs. The commercial DC analyzer was found to be virtually useless below 0.5 mrad, but the photon counter maintained good linearty and accuracy over this range. Finally, as a means of testing the photon counting system's response for very low dose levels, the absorbed dose due to background was measured at two hour intervals using the ^{7}LiF TLDs and a set of CaF_2:Mn (TLD-400) TLD rods. This was equivalent to measuring dose intervals equal to approximately 15.6 μrads. Both sets of TLDs produced data with good linearty for such small doses. The results obtained with CaF_2:Mn showed slightly better linearity and smaller standard deviations within each subset of TLDs.